2003

Theoretical models of many-quark bound states

Richard Jeffrey Lloyd
Iowa State University

Theoretical models of many-quark bound states

by

Richard Jeffrey Lloyd

A dissertation submitted to the graduate faculty

in partial fulfillment of the requirements for the degree of

DOCTOR OF PHILOSOPHY

Major: Nuclear Physics

Program of Study Committee:
James P. Vary, Major Professor
John C. Hill
Jianwei Qiu
Kerry L. Whisnant
Glenn R. Luecke

Iowa State University

Ames, Iowa

2003

ProQuest Information and Learning Company
300 North Zeeb Road
P.O. Box 1346
Ann Arbor, MI 48106-1346

Graduate College
Iowa State University

This is to certify that the doctoral dissertation of

Richard Jeffrey Lloyd

has met the dissertation requirements of Iowa State University

Signature was redacted for privacy.

Major Professor

Signature was redacted for privacy.

For the Major Program

TABLE OF CONTENTS

ABSTRACT

The foundations of Many-Fermion Dynamics (MFD) are developed with special attention paid to a treatment of color and flavor degrees of freedom. From these ingredients a framework was developed to calculate the properties of many-fermion bound states. The quark implementation of MFD (MFDq) was extensively tested on the 2-body problem against the established nucleon implementation of MFD (MFDn). We were able to perform a limited set of self-consistency checks of MFDq in the 4-body problem to test a proper treatment of all computed matrix elements.

Finally, calculations are presented using MFDn to predict the properties of 4-body charmonium bound states. With MFDn, we find a lowest bound state of J=0 at about 6.033 GeV with a deviation of .084 GeV. Additional bound states are also obtained. Preliminary calculations with MFDq qualitatively confirm these results.

1 A BRIEF OVERVIEW OF EXOTIC CANDIDATES

Introduction

Quantum Chromodynamics (QCD) has become widely accepted as the theory of the strong interactions and has gained a stature close to that of Quantum Electrodynamics (QED) due to its predictive power. QCD provides us with a theory of quarks interacting via gluon exchange in a manner somewhat analogous to QED providing a theory of charged particles interacting via the exchange of photons. One major difference is that the gluons are self-interacting whereas photons are not. Another major difference is that the predictive power of QCD is mainly limited to the perturbative regime where high momentum transfers are involved. The regime of strong interaction bound states and low energy scattering (e.g. resonances), or low-momentum physics, is yet to be adequately addressed in the QCD framework.

In the absence of direct predictions for bound states and resonances from QCD, one relies on models inspired by QCD. The dominant models for mesons and baryons are the constituent quark models. In a constituent quark model one uses massive quarks interacting through effective potentials modeled from QCD. The effective interactions account for gluon exchange between the quarks and antiquarks. The resulting description of few-quark systems (quarks and antiquarks) is the main focus of this investigation.

In this chapter we introduce the necessary terminology to classify the various kinds of exotic bound states believed to arise in QCD. "Exotic" generically refers to a bound state that is not a simple meson well approximated as a quark-antiquark ($q\bar{q}$) or a simple baryon well approximated as a three-quark (qqq) system. We then discuss a few of the experimental candidates for exotic states found in the literature and indicate some of the current models used to calculate the properties of these states. We will not undertake,

however, a systematic inter-comparison of these models although a limited comparison of our own approach to some of these models will be given in Chapter 5 of this work.

The present study deals with only one kind of exotic bound state, that of a many-quark system (including antiquarks). We realize and acknowledge that this type of exotic state has not yet been convincingly identified in experiments. In fact, other types of exotic states may well be far more common. However, this determination may rest on an incomplete understanding of the experimental evidence. In any case a clear and consistent theoretical description of many-quark bound states and their properties will go a long way toward sharpening these issues, some of which we will outline in this chapter.

The Nomenclature of Exotic States

As we have already noted in the introduction, exotic states are those which can not be described as a conventional meson or baryon though they may have the same quantum numbers. Many abbreviated [1] and some more elaborate overviews [2,3] of exotic classifications and candidates are common. The four main categories of exotics are labeled glueballs, hybrids, exotic mesons and many-quark states. These classifications may not be mutually exclusive. In fact the use of "exotic" as an overall label for this group of states and also for a sub-category is sometimes confusing but we hope that the context will make clear the usage to which we refer.

Glueballs are in the meson sector and consist of bound states of gluons with little or no $q\bar{q}$ content. The two lightest glueballs are theoretically expected to be the scalar $J^{PC} = 0^{++}$ and the tensor $J^{PC} = 2^{++}$ state with masses of about 1.6 GeV and 2.3 GeV, respectively [4,5]. Some candidates have been identified and will be more fully discussed in a later section.

Hybrid states are hadrons (meson or baryon) that have an excited glue component [2]. Some hybrid mesons may be identified by their "non-$q\bar{q}$" quantum numbers $J^{PC} = 0^{--}, 0^{+-}, 1^{-+}, 2^{+-}$ ...etc., where J is the total angular momentum, P is the parity and C is the charge conjugation quantum number of the bound state. We should note that mesons are

not generally eigenstates of C unless they are their own antiparticles. For a meson, the quark model predicts that $P = (-1)^{L+1}$ and $C = (-1)^{L+S}$ where L is the orbital angular momentum and S is the spin of the meson. Since we know that $|L-S| \leq J \leq L+S$, this implies that the J^{PC} assignments just enumerated for the hybrid states are forbidden to simple mesons ($q\bar{q}$ systems). Hence, the appearance of states with forbidden quantum numbers in the meson spectrum is a sure sign of an exotic state. However, hybrid states can also have the same quantum numbers as a meson, and any exotic state with this feature is sometimes called cryptoexotic. Detection of these states may rely on unusual decay channels or other properties difficult to explain with a $q\bar{q}$ quark model. To date, two relatively good candidate hybrid mesons have been found [2], but no firm candidates have been identified in the hybrid baryon system. Since there are no exotic J^P baryons, they must be identified in some other way. The experimental signatures for an exotic baryon are an overpopulation of the baryon spectrum or unusual couplings in their decay channels [6]. These constitute signatures since a hybrid baryon represented by a state like a $|qqqg\rangle$ multiplet does not span the same space as multiplets in the pure baryon sector, $|qqq\rangle$, leading to an apparent "overpopulation" of baryon states.

Exotic mesons have J^{PC} quantum numbers forbidden to simple mesons and hence the underlying structure of these particles does not have any pure $|q\bar{q}\rangle$ component. It is usually considered to be a linear combination of $|q\bar{q}g\rangle, |gg\rangle, |q^2\bar{q}^2\rangle$, etc. Note that this definition subsumes the classifications of some hybrid and glueball candidates. We will retain these other classifications for the purpose of being definite in our discussions. Two strong candidates for an exotic meson have been found [2] and will be discussed later.

"Many-quark states" is a collective label for any state that is completely dominated by quark constituents. Many-quark states include dibaryons, 2 quark-2antiquark systems and any other combination of quarks and/or antiquarks that may have a global color singlet structure. To date there is some evidence that suggests these kinds of states have been

found, mainly due to some experimentally well-known resonances that can not be completely ruled out as belonging to this class of exotics.

In what remains of this chapter, we will give a brief discussion of each type of exotic and its experimental candidates. Then we will give a cursory description of some models in the theoretical literature that seeks to predict the properties of these exotics.

Glueball Candidates

There are three known states not easily incorporated into the quark model that are considered glueball candidates or states with a large glue component. These are the scalar and J-mesons $f_0(1500), f_0(1710), f_J(2220)$. The physics community according to an elaborate set of rules assigns the names for these states. The masses of the states are quoted in parentheses in units of MeV.

The scalar meson $f_0(1500)$ is considered to be a candidate for the $J^{PC} = 0^{++}$ glueball, although the $f_0(1710)$ is also a contender [3].These determinations are based primarily on the decay channels of these states where the $f_0(1710)$ decays mainly into $K\overline{K}$ which indicates it has a significant $s\bar{s}$ structure. The $f_0(1500)$ does not often decay to $K\overline{K}$ or $\pi\pi$, and the branching ratio of the $K\overline{K}$ channel as compared to the $\pi\pi$ is small, indicating that $f_0(1500)$ is probably not an $s\bar{s}$ structure. Additionally, the $f_0(1500)$ has a narrow decay width and tends to be produced in glue-rich environments. This lends credence to the possibility of a glueball or at least a glue-dominated state.

The tensor glueball with $J^{PC} = 2^{++}$ is very tentatively identified with the $f_J(2220)$, although this has been called into question [7]. The evidence conflicts in a decay channel analysis. Essentially, there is an enhancement in the $\varphi\varphi$ cross section in $p\bar{p}$ collisions that may be attributable to $J^{PC} = 2^{++}$ glueball production. On the other hand, partial widths of J/ψ are not consistent with upper limits of $\pi\pi$ production in $p\bar{p}$ annihilation [7]. Hence this identification is not at all firm.

Hybrid Candidates

Hybrid candidates are often taken to be nearly synonymous with exotic J^{PC} mesons. This occurs because, typically, there are few other viable candidates consistent with both experimental evidence and theoretical models other than hybrids that would produce a J^{PC} exotic meson. An exotic meson is simply a state with exotic J^{PC}. A hybrid, on the other hand, could have any J^{PC} whatsoever. Obviously these categories overlap, but each has its own unique domain. Exotic mesons include 4-quark candidates without glue component while hybrids do not. Also exotic mesons could be quasi-bound nuclear (or molecular) states that could not be called hybrid. In any case, we shall treat these cases separately, with exotic mesons to be dealt with later. It turns out however, that the only established exotic meson candidates are also widely regarded to be hybrids with high probability.

The Exotic Mesons

The best-established exotic meson has been designated the $\pi_1(1600)$, and another candidate the $\pi_1(1400)$, formerly the $\hat{\rho}(1405)$, are quite viable [2]. Both of these states have been determined to have exotic $J^{PC} = 1^{-+}$. Neither of these states can be glueballs, the lightest of which are expected to be heavier than these masses and have very different J^{PC} assignments than either of these candidates. The $\pi_1(1600)$ is favored to be a hybrid since it strongly couples to $\eta'\pi$ but not $\eta\pi$ via decay, while the $\pi_1(1400)$ couples to $\eta\pi$ via decay. This leads to a sentiment that the $\pi_1(1600)$ is a hybrid while the $\pi_1(1400)$ may be a 4-quark state.

One objection to the identification of the $\pi_1(1600)$ as a hybrid is that the reported mass differs significantly (about 300 MeV) from theoretical predictions. Also the decay patterns, especially the decay to $\eta'\pi$ are very inconsistent with models for hybrid decays [8,9].

Whether this is simply a deficiency in the theoretical models or an unanticipated difficulty in the data analysis or experimental detection is not entirely settled.

The $\pi_1(1400)$ has also been clearly identified in the experimental results (e.g. [10]), but again a light, broad state is difficult to explain in theoretical models that predict a hybrid state would be several hundred MeV heavier and the width in the $\eta\pi$ channel much narrower than is found.

The Many-Quark States

The resonances best supported by experiment to be many-quark states are probably the $f_0(980)$ and the $a_0(980)$. Both states have a propensity to decay to $K\overline{K}$ which suggests they may be $K\overline{K}$ molecular states, loosely bound configurations of $K\overline{K}$ [3]. However, since their masses are so close to the $K\overline{K}$ threshold, and their widths allow either state to straddle this threshold, it is difficult to characterize conclusively either of these states. Some measurements have been proposed to nail down the constituents of these states [11], primarily by examining the branching ratios to determine the strange quark content in the $\varphi \to f_0\gamma$ and $\varphi \to a_0\gamma$ channel since the magnitude of these ratios are sensitive to the final state quark content. To date, these measurements have not been completed.

There are several candidates we have not mentioned. This is not due to the fact that we have a particular prejudice in favor of the ones that have been examined here; rather it reflects our judgement about the level of certainty in the literature about the viability of these candidates relative to others we have mentioned. In order to illustrate the general stature of candidates we have not explicitly examined, we shall introduce a candidate that was reported only recently [12]. A narrow state found at BABAR was reported and tentatively identified as $J^P = 0^+$ with a mass of about 2.32 GeV. In the quark model this could only be a $c\bar{s}$ state, but the decay width is narrower and the mass lower than predicted by potential models of these states. The authors of the experimental paper conclude, tentatively, that it may be a 4-quark system based on the inability of theoretical quark and

other exotic models to account for the properties of the reported state. Beyond this statement there is no firm determination of the particular content of this state.

Since this result is preliminary, its status should not be given the same weight as other candidates that have been reported, often in several different experiments, like the candidates we have examined in brief detail above. It may happen however that the result will withstand further analysis and become a very strong candidate for another exotic state in the meson spectrum.

Theoretical Models

There are a wide variety of possible exotic states and there are a great number of theoretical models that seek to understand and predict their properties. Here we give only a cursory review of the popular models of exotic states and a brief outline of their strengths.

Some of the earliest theories of exotic states were bag models of hybrid states [4,5] and their improvements [13,14]. These models typically consist of relativistic massless quarks and gluons interacting through various potentials in a fixed external spherical cavity. Decays are usually ignored in the search for stable hybrid states of quarks and gluons. These approaches have been applied to the hybrid baryon problem, but so far no experimental candidates for a hybrid baryon have been found. Given this dearth of experimental confirmation, it is difficult to gauge the success of these models in the baryon sector. They have had moderate success in predicting the properties of some of the exotic candidates reviewed earlier, especially recent estimates of the exotic meson masses. Other properties, however, such as the decay widths and decay modes are still poorly understood.

A major distinguishing feature between bag models and our own approach is the treatment of center of mass (CM) motion. Since the bag models invoke a fixed external cavity they are not translationally invariant. Our approach is translationally invariant, as we believe that spurious CM motion effects may be large in few-body problems. On the other hand, the bag models treat the motions relativistically while we adopt a non-relativistic approach with relativistic corrections to be applied at a later stage.

The flux tube model [15] seeks to model hybrids with an excited "gluon flux tube" that mediates interactions between quarks. There is some agreement between this model and lattice gauge theory, where both predict the lightest exotic J^{PC} meson to be about 1.9-2.0 GeV. Also the flux tube model reproduces some of the predictions of the bag model, namely the Roper resonance, although the flux tube model gives a higher mass and doubles the degeneracy. As of yet, the flux tube model has not been extended to predict decay amplitudes of the strong interaction—i.e. the dynamics of flux tube breaking to produce multiparticle final states has not been done.

Lattice gauge theory represents the most promising approach since it originates directly from QCD, the fundamental theory of the strong interactions. However, it is computationally very intensive—requiring the most advanced computers running for very extended periods of time, even years. Our own approach maintains computational simplicity by comparison.

Earlier [17] and more recent reviews [16,19] show that lattice QCD can be applied to a wide number of problems in the exotic spectrum, including exotic mesons, hybrids and glueballs. At present lattice theory predicts the spectra of many of these states. There are technical complications in the heavy meson spectra however, since the lattice spacing attainable in current calculations is larger than the quark masses themselves. The only way around this difficulty at present is to use an effective Lagrangian approach. The predictions of the candidate glueball and exotic meson masses and other properties are roughly concordant with the candidates known from experiment.

Among the differences between the lattice approach and our own, we mention that the lattice method, like the bag models, does not preserve translational invariance. On the other hand, the lattice method preserves gauge invariance while our method is based on a particular but popular gauge choice, and we have not yet assessed the possible gauge dependence of our method. Furthermore, the lattice method is relativistic while our approach, as previously mentioned, is non-relativistic at present.

Several approaches exist in the literature that have gone unmentioned so far. For example, a Bethe-Salpeter approach to exotic mesons is contained in Ref. [18] that gives

reasonable fits to the candidates described earlier and others that were not discussed in this thesis.

Also, a dispersion relation technique [20] that has been recently applied to compute the properties of a pentaquark system ($qqqq\bar{q}$) is another approach. This treatment is based on N-body relativistic generalizations of the Fadeev-Yakubovsky equations [21,22]. The model presently assumes SU(3) flavor symmetry in the light quark sector which is not entirely realistic.

In order to examine questions of fundamental significance with minimal limitations due to our non-relativistic approach, we will focus on heavy quark systems—specifically the charmed quark sector in the present work. The charm quarks with masses around 1.5 GeV have long been modeled with non-relativistic approaches as the effects of relativity are expected to be much smaller than in lighter quark systems. Hence, we hope to have maximum predictive power for a portion of the meson spectrum, including many-quark exotics, where present experimental efforts may provide new discoveries. It is important to note that, to our knowledge, no experimental or theoretical evidence has been presented before the present work on the possible existence of exotic multi-charmonium systems.

Summary and Conclusions

We have seen that the exotic candidate spectrum is varied and quite complicated. Indeed, it is even more complicated than we have represented here, confining ourselves only to the best understood candidates in the literature.

The models used to describe the exotic spectrum are equally varied, although lattice gauge theory seems to have the potential for giving a unified treatment of all states in QCD though it is unclear how the fundamental issue of translational invariance will ever be resolved in this framework. Having a single successful approach, such as lattice QCD, certainly would be a relief given the plethora of specialized approaches, each of which must make some rather strong assumptions about the constituents of exotic states even before the calculations begin. Although this may sound critical, the author realizes the magnitude of

the problem at hand. In fact, the approach presented in this thesis makes its own assumptions when we restrict ourselves only to many-quark candidates with no explicit glue component. That is, we treat gluons as essentially integrated out into the effective interactions among the quark degrees of freedom. The subset of the exotic spectrum that we address may, depending on interpretation of the current state of theory, turn out to be the least promising if some researchers are to be believed [19]. Their conclusion rests mainly on inferences drawn about the light quark sector of the exotic meson spectrum, and in this thesis we will exclusively investigate the charm sector of the multi-quark states, the charm quark being the lightest "heavy quark".

We aim, in the remainder of this thesis, to expound the background and detail necessary to understand the power of the approach of Many-Fermion Dynamics (MFD), the main framework developed here to understand the bound states of many-quark systems. We shall also present initial results for multi-quark systems (exotics) with various Hamiltonians modeled to reproduce the experimental spectra of $c\bar{c}$ systems.

The results we present are unique in that they address multi-quark charmed mesons that, to our knowledge, have not previously been addressed in the literature. We are excited by the prospect that such exotic systems may be discovered and examined in detail at the Relativistic Heavy Ion Collider (RHIC) using the PHENIX detector. It should be mentioned that Iowa State University is a leader in the PHENIX experiments at RHIC.

References

[1] Particle Data Group, Eur. Phys. J. C **15**, 682 (2000).

[2] T. Barnes, Acta Phys. Polon. **B31**, (2000) 2545-2556.

[3] S. Godfrey and J. Napolitano, Rev. Mod. Phys. **71**, 1411 (1999).

[4] N. Isgur, R. Kokoski and J. Paton, Phys. Rev. Lett. **54**, 869 (1985).

[5] T. Barnes, F. E. Close and E. S. Swanson, Phys. Rev. D **52**, 5242 (1995).

[6] T. Barnes, *Hybrid Baryons, A brief review*, nucl-th/0009011 v1. (2000).

[7] C. Amsler, Nuc. Phys. **A663**, (1999).

[8] N. Isgur, Phys. Rev. Letters **54**, 869 (1985).

[9] F. E. Close and P. R. Page, Nucl. Phys. **B443**, 233 (1995)

[10] D. R. Thompson et al., Phys. Rev. Lett. **79**,1630 (1997).

[11] F. E. Close, N. Isgur and S. Kumano, Nucl. Phys. **B389**, 513 (1993).

[12] B.Aubert et al., hep-ex/0304021 v1, (2003).

[13] C. E. Carlson, T. H. Hansson and C. Peterson, Phys. Rev. **D27**, 1556 (1983).

[14] E. Golowich, E. Haqq and G. Karl, Phys. Rev. **D33**, 859 (1986).

[15] N. Isgur and J. Paton, Phys. Rev. **D31**, 2910 (1985).

[16] K. Chetrykin and S. Narison, Phys. Lett. **B485**, 195 (2000).

[17] J. I. Latorre, P. Pascual and S. Narison, Z. Phys. **C34**, 347 (1987).

[18] C. J. Burden and M. A. Pichowsky, Few Body Systems **32**, 117 (2002).

[19] C. McNeile, Nucl. Phys. **A711**, 303 (2002).

[20] S. M. Gerasyuta and V. I. Kochkin, hep-ph/0211436.

[21] S. M. Gerasyuta, Nuovo Cim. **A106**, 37 (1993).

[22] S. M. Gerasyuta, Z. Phys. **C60**, 683 (1993).

2 MANY-QUARK STATES IN FLAVOR AND COLOR SPACE

Introduction

In making a realistic model to calculate many-quark bound states, there are several ingredients to be considered. The first and most fundamental of these is the color degree of freedom that is characterized by an SU(3) symmetry that will be discussed in detail in this chapter. This feature deserves careful attention in many-quark systems since it is well known from group theory that systems with more than three quarks may allow for more than one color singlet. This is important since color singlets are believed to be the only bound states that are physically realizable. Any other bound state is termed "exotic" as outlined in Chapter 1. When studying mesons (treated here as $q\bar{q}$) and baryons (qqq systems) the intrinsic color structures may be ignored because each of these cases admits only one color singlet.

This chapter will introduce the mathematics of Lie groups [1,2], particularly of SU(3) color. Then a toy model which incorporates SU(2) flavor and SU(2) color will be introduced in order to illuminate certain issues in many-body states that involve both the color and flavor degrees of freedom. Eigenstates of color and flavor will be constructed from group theory arguments and, after antisymmetrization, will be used to answer questions regarding the multiplicity of states. A few simple Hamiltonians will then be employed to raise questions concerning the potential mixing of the color singlets and the meaning of "color exotic" in the many-quark picture.

The Mathematics of SU(3) Color

The properties of SU(3) depends entirely on the group generators, particularly their commutation relations as defined below.

$$[\lambda_k, \lambda_l]_- = \lambda_k\lambda_l - \lambda_l\lambda_k = 2if_{kln}\lambda_n \tag{2.1}$$

The λ_i and the f_{kln} are the traceless SU(3) group generators and the totally antisymmetric structure constants, respectively, and i=1,2,...,8 is a color label. The anti-commutation relations are as follows.

$$[\lambda_k, \lambda_l]_+ = \lambda_k\lambda_l + \lambda_l\lambda_k = 2d_{kln}\lambda_n + \frac{4}{3}\delta_{kl} \tag{2.2}$$

The d_{kln} are totally symmetric constants under exchange of indices, and δ_{kl} is the Kronecker delta which is defined as follows:

$$\delta_{ij} = \begin{cases} 1, & i = j \\ 0, & i \neq j \end{cases}$$

Table 7.1 of Ref. [7] lists the symmetric and antisymmetric coefficients defined in equations 2.1 and 2.2. Other properties of the group generators are recorded here for reference purposes.

$$\mathrm{Tr}(\lambda_i\lambda_j) = 2\delta_{ij}$$

$$\mathrm{Tr}(\lambda_k) = 0, \quad \forall k$$

Using these definitions and properties, two Casimir operators can be defined, although only one of them is really necessary, as we shall see [7].

$$C_1 = \frac{1}{4}\sum_{i=1}^{8}\lambda_i^2$$

$$C_2 = \frac{1}{8}\sum d_{ijk}\lambda_i\lambda_j\lambda_k = C_1\left(C_1 - \frac{11}{6}\right)$$

It is obvious that the second Casimir operator is just a simple quadratic polynomial of the first Casimir operator and therefore redundant for our purposes. One other fact that we shall use frequently is that any SU(N) group has N-1 diagonal generators [7]; for SU(3) the eigenvalues of these diagonal generators are designated by Y and I^3, the "color hypercharge" and "color isospin" respectively.

It will be advantageous in our study of many fermion systems if we can classify and construct color states in an efficient manner, particularly the color singlets. We shall define an 8-vector in color space in analogy to the SU(2) spin model to help with this task, and use the convention that color unit vectors are implicit:

$$\vec{\lambda} \equiv \sum_{i=1}^{n}\vec{\lambda}_i = \sum_{a=1}^{8}\sum_{i=1}^{n}\lambda_i^a$$

The particle labels are now the lower indices, and the color labels are the upper indices, following the common practice in standard treatments of the subject [7]. If we take the dot product of this expression with itself we will find after some rearrangement the following useful formula:

$$\sum_{i<j}^{n}\vec{\lambda}_i \bullet \vec{\lambda}_j = \frac{1}{2}\left(\vec{\lambda}^2 - \sum_{i=1}^{n}\vec{\lambda}_i^2\right) \qquad (2.3)$$

The eigenvalues of the operator defined in equation 2.3 enable us to classify color multiplets based on the eigenvalues we obtain by diagonalization in any many-body problem. Moreover, $\vec{\lambda}^2 = 0$ for a color singlet, and is positive for every other multiplet. The operator on the left-hand side of equation 2.3 has the lowest eigenvalue for a color singlet. Hence we

only need choose the associated eigenvectors of the most negative eigenvalue of a system that allows a color singlet and we may be assured that it is a color singlet. The second term in parentheses in equation 2.3 simply provides an additive constant that depends only on the particle number.

The construction of color eigenstates proceeds in a fairly simple manner. Since each quark has three possible color states, combinatorial issues quickly make prohibitive demands. We can minimize this difficulty by employing the diagonal generators Y and I^3, mentioned previously. Table 2.2 gives the values for these generators for each quark "color" below. Fortunately, we only need retain many-body states that meet the following criteria (recall that lower indices refer to particle labels):

$$\sum_{i=1}^{n} Y_i = 0$$
$$\sum_{i=1}^{n} I_i^3 = 0 \qquad (2.4)$$

It should be noted that states other than color singlets will meet these criteria, but we may still distinguish between these states and the color singlets by the eigenvalues of the operator defined in equation 2.3. This procedure is implemented for computational efficiency. For example in a meson system, only 3 of the possible 9 color combinations need be considered; for a baryon only 6 of the 27 possible combinations; for a $2q2\overline{q}$ exotic state, only 15 of the possible 81 color combinations need be included. This drastically reduces the computer storage space necessary for realistic many-body calculations.

Table2.2: Color isospin, I^3, and color hypercharge, Y, for each quark.[a].

Color	Y	I^3
Red(r)	1	1
Green(g)	1	-1
Blue(b)	-2	0

[a] Negatives of the above values yield the quantum number assignments for antiquarks.

The color charge is defined to be $Q = I^3 + \frac{Y}{2}$, and equation 2.4 this implies that we select states with zero total color charge by. With these preliminaries in place, we are in a position to compute the matrix elements of the operator defined in equation 2.3. We must choose a basis for expressing the matrix elements systematically. A product space basis of single particles states motivated by Figure 2.1, a Feynman diagram for a one gluon exchange between colored fermions, is convenient. The indices i, j, k, and l are color labels for the quarks, and the other labels are described in the text following the diagram.

Figure 2.1: Feynman diagram for one gluon exchange between quarks

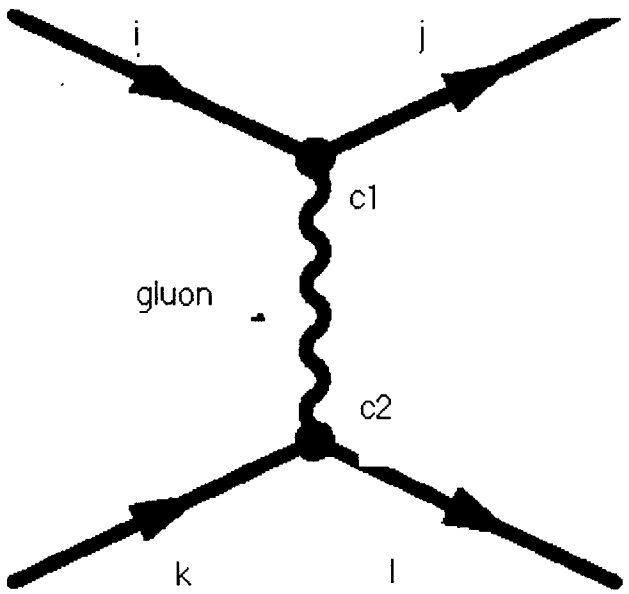

In Figure 2.1 we will use the convention that time is running left to right as noted by the arrows on the quark (heavy straight lines). According to the Feynman rules for evaluating the matrix elements, there is an operator associated with each vertex in the diagram. These operators, c1 and c2, are defined below in the product space as matrix elements of the SU(3) generators. $\hat{i}$ is the pure imaginary number of unit magnitude.

$$c1 = \hat{i}\langle j|\hat{\lambda}|i\rangle \equiv \hat{i}\lambda_{ij}$$
$$c2 = -\hat{i}\langle l|\hat{\lambda}|k\rangle \equiv -\hat{i}\lambda_{kl}$$

The product of c1 and c2 is the same operator in different guise defined in equation 2.3. Matrix elements of that operator can now be expressed in the notation just introduced where i and k (j and l) refer to the colors of the incoming (outgoing) quarks. From Ref. [3], the product space matrix elements for two incoming quarks and two outgoing quarks are given for any SU(N) generators by the following expression.

$$\lambda_{ij}\lambda_{kl} = \frac{1}{2}\left(\delta_{il}\delta_{kj} - \frac{1}{N}\delta_{ij}\delta_{kl}\right) \tag{2.5}$$

For the case of color, N=3, but this expression is equally useful for any SU(N) group generators, including flavor. The matrix elements for incoming and outgoing $\overline{q}\overline{q}$ are exactly the same as in equation 2.5. The case of incoming and outgoing $q\overline{q}$, however, is different. If, for example, we let the lower line in Figure 2.1 refer to $\overline{q}$ and the upper line to q, the factor c2 must be replaced with $c2^*$, where $c2^*$ is the complex conjugate of c2. However, the group generators are Hermitian [7,8], and this allows us to substitute the transpose of c2 for $c2^*$. These considerations yield the $q\overline{q}$ matrix element. For pedagogical purposes we record the result here.

$$\lambda_{ij}\lambda^{T}{}_{kl} = -\frac{1}{2}\left(\delta_{ik}\delta_{lj} - \frac{1}{N}\delta_{ij}\delta_{kl}\right)$$

In what follows we shall develop a toy model that employs these features to address the questions stated in the Introduction. For simplicity, however, we shall use SU(2) symmetry for both flavor and color. This approach affords some shortcuts, we believe, without sacrificing the pedagogical benefits.

A 4-Body Toy Model Using SU(2) in Flavor and Color Space

The model chosen is a $2q2\bar{q}$ system of $SU(2)_f \otimes SU(2)_c$ where "f" stands for flavor and "c" for color. Our goal is to construct a maximal set of orthogonal, antisymmetrized 4-body states in order to address some of the questions raised in the introduction. The flavors are denoted by u and d, the colors by r and b. We shall assume that the u and d quarks belong to a flavor doublet obeying SU(2) symmetry, and an exactly analogous color doublet, also obeying SU(2) symmetry.

We desire to couple the particles and antiparticles in our toy problem using the same phases for the Clebsch-Gordon coefficients for particles and antiparticles. For this purpose, we adopt the convention that the particle (or antiparticle) with the largest positive electric charge occupies the upper member of the doublet as in Ref. [4]. We shall develop this ingredient explicitly for flavor since color is exactly analogous. The particle doublet appears as follows with these conventions.

$$\begin{pmatrix} u \\ d \end{pmatrix}$$

The u quark has electric charge 2/3 and $F^3 = 1/2$ while the d quark has charge $-1/3$ and $F^3 = -1/2$. (F^3 is the third component of the SU(2) flavor operator F.) If we simply applied the charge conjugation operator to the doublet we would have the upper member of the resulting antidoublet with the negative charge, violating the usual convention. To preserve the convention we will reorder the members of the antidoublet, but this raises the possibility that we introduce a phase when we do so. To fix this phase, we reason that reordering the antidoublet is equivalent to doing a rotation of π on the charge-conjugated doublet about the 2-axis. Hence, if the rotation operator acts on the charge-conjugated doublet, any phase that appears will be immediately apparent:

$$e^{-i\pi\tau_2/2}\begin{pmatrix}\bar{u}\\ \bar{d}\end{pmatrix}=-i\sigma_2\begin{pmatrix}\bar{u}\\ \bar{d}\end{pmatrix}=\begin{pmatrix}0 & -1\\ 1 & 0\end{pmatrix}\begin{pmatrix}\bar{u}\\ \bar{d}\end{pmatrix}=\begin{pmatrix}-\bar{d}\\ \bar{u}\end{pmatrix} \tag{2.6}$$

σ_2 is the usual Pauli matrix [4]. (The relation follows since any even power of any Pauli matrix is the identity.) The extra phase for the upper member of the rotated, charge-conjugated doublet motivates using 2.6 to define the antidoublet. It satisfies all the requirements noted earlier; namely, the upper member of the antidoublet has the most positive charge (1/3), and clearly the antidoublet has the same properties under rotations as the doublet. Using the conventional rules for Clebsch-Gordon coupling, we can now construct states with arbitrary numbers of particles and antiparticles. Following are the possible 2-body particle-antiparticle states of flavor using the established conventions:

$$\left.\begin{aligned}&|F=1,F^3=1\rangle=-u\bar{d}\\ &|F=1,F^3=0\rangle=\frac{1}{\sqrt{2}}\left(u\bar{u}-d\bar{d}\right)\\ &|F=1,F^3=-1\rangle=d\bar{u}\end{aligned}\right\}\quad\text{triplet}$$

$$\left.|F=0,F^3=0\rangle=\frac{1}{\sqrt{2}}\left(u\bar{u}+d\bar{d}\right)\right\}\quad\text{singlet} \tag{2.7}$$

Color follows a similar treatment, and the color eigenstates can be constructed by making the substitution u→r, and d→b, replacing the flavor labels with color labels.

We can now construct 4-body states of color and flavor. The flavor states will be done explicitly since the color construction is the same in accordance with Ref [5]. (Furthermore, we shall restrict ourselves to color singlets only, but place no such restrictions on flavor.) The results for the flavor states are shown below. As a pedagogical note, we should point out that flavor triplet states are by far the most numerous eigenstates that emerge from coupling to the 4-body states. We will see that this will not remain the case after antisymmetrization.

$$\left.\begin{aligned}
&\left|F=2,F^3=2\right\rangle = u\bar{d}u\bar{d}\\
&\left|F=2,F^3=1\right\rangle = -\frac{1}{2}[u\bar{d}(u\bar{u}-d\bar{d})+(u\bar{u}-d\bar{d})u\bar{d}]\\
&\left|F=2,F^3=0\right\rangle = \frac{1}{\sqrt{6}}[(u\bar{u}-d\bar{d})(u\bar{u}-d\bar{d})-d\bar{u}u\bar{d}-u\bar{d}d\bar{u}]\\
&\left|F=2,F^3=-1\right\rangle = \frac{1}{2}[(u\bar{u}-d\bar{d})d\bar{u}+d\bar{u}(u\bar{u}-d\bar{d})]\\
&\left|F=2,F^3=-2\right\rangle = d\bar{u}u\bar{d}
\end{aligned}\right\} \text{ quintuplet} \qquad (2.7a)$$

$$\left.\begin{aligned}
&\left|F=1,F^3=1\right\rangle_{tt} = \frac{1}{2}[(u\bar{u}-d\bar{d})u\bar{d}-u\bar{d}(u\bar{u}-d\bar{d})]\\
&\left|F=1,F^3=0\right\rangle_{tt} = \frac{1}{\sqrt{2}}[d\bar{u}u\bar{d}-u\bar{d}d\bar{u}]\\
&\left|F=1,F^3=-1\right\rangle_{tt} = \frac{1}{2}[(u\bar{u}-d\bar{d})d\bar{u}-d\bar{u}(u\bar{u}-d\bar{d})]
\end{aligned}\right\} \text{ triplet}$$

$$\left.\begin{aligned}
&\left|F=1,F^3=1\right\rangle_{ts} = -\frac{1}{\sqrt{2}}u\bar{d}(u\bar{u}+d\bar{d})]\\
&\left|F=1,F^3=0\right\rangle_{ts} = \frac{1}{2}(u\bar{u}-d\bar{d})(u\bar{u}+d\bar{d})\\
&\left|F=1,F^3=-1\right\rangle_{ts} = \frac{1}{\sqrt{2}}d\bar{u}(u\bar{u}+d\bar{d})]
\end{aligned}\right\} \text{ triplet} \qquad (2.7b)$$

$$\left.\begin{aligned}
&\left|F=0,F^3=0\right\rangle_{tt} = -\frac{1}{\sqrt{3}}[u\bar{d}d\bar{u}+dd\bar{u}u\bar{d}+(u\bar{u}-d\bar{d})(u\bar{u}-d\bar{d})] \equiv \left|X_E^F\right\rangle\\
&\left|F=0,F^3=0\right\rangle_{ss} = \frac{1}{2}(u\bar{u}+d\bar{d})(u\bar{u}+d\bar{d}) \equiv \left|X_0^F\right\rangle
\end{aligned}\right\} \text{ singlets}$$

There are other triplet states, shown below, that form flavor eigenstates. The subscripts on the flavor 4-body triplet and singlet states refer to how the 2-body states were coupled to construct the states above. (tt refers to triplet-triplet 2-body coupling, ts to triplet-singlet, and ss to singlet-singlet coupling.) There is also a singlet-triplet coupling, which produces a flavor triplet state. It is recorded below for completeness.

$$\left.\begin{aligned}
\left|F=1,F^3=1\right\rangle_{st} &= -\frac{1}{\sqrt{2}}(u\bar{u}+d\bar{d})u\bar{d} \\
\left|F=1,F^3=0\right\rangle_{st} &= \frac{1}{2}(u\bar{u}+d\bar{d})(u\bar{u}-d\bar{d}) \\
\left|F=1,F^3=-1\right\rangle_{st} &= \frac{1}{\sqrt{2}}(u\bar{u}+d\bar{d})d\bar{u}
\end{aligned}\right\} \quad \text{triplet} \qquad (2.7c)$$

The two color states we allow are the color singlets, the color analogues of the flavor singlet states in equation 2.7b. In the case of color, $\left|X_0^C\right\rangle$ is a "2-meson" color state, and $\left|X_E^C\right\rangle$ is the "exotic" color singlet, both analogues of the flavor singlets in 2.7b. The full 4-body states are now just simple tensor products of the flavor eigenstates in 2.7a-c with the color singlet eigenstates.

$$\left|\Psi\right\rangle = \left|F,F^3\right\rangle \otimes \left|C=0,C^3=0\right\rangle \qquad (2.8)$$

Note that C=0 as does the third component of C, in order to require that only global color singlet states be retained in accordance with all present experimental evidence.

Let us now define an operator, the antisymmetrizer, as follows [6].

$$A\left|\Psi(1,2,3,4)\right\rangle = \frac{1}{\sqrt{n!m!}}\sum_P \varepsilon_P \left|\Psi\left[\hat{P}(1,2,3,4)\right]\right\rangle \qquad (2.9)$$

$\hat{P}$ denotes the permutation operator of identical fermions and ε_P is 1 (-1) if the permutation is even (odd). $\hat{P}$ does not exchange non-identical fermions. This is reflected in the statistical factor in 2.9, which normalizes the sum. (The factors n and m equal the numbers of each species of particle that are represented in the wave function. In our present case n=m=2.) If we take all tensor products of flavor states in equations 2.7a-c with the two possible color states as described by 2.8 and apply equation 2.9 to the results, we form 10 linearly independent states. An example of applying equation 2.9 to obtain antisymmetric states will be carried out explicitly for the F=2 case with a maximal third component of F.

$$A|\Psi\rangle = A\left[u\bar{u}d\bar{d}\frac{1}{2}\left(r\bar{r}r\bar{r} + b\bar{b}b\bar{b} + r\bar{r}b\bar{b} + b\bar{b}r\bar{r}\right)\right]$$
$$= \frac{1}{4}u\bar{u}d\bar{d}[\left(r\bar{r}r\bar{r} + b\bar{b}b\bar{b} + r\bar{r}b\bar{b} + b\bar{b}r\bar{r}\right)$$
$$-\left(r\bar{r}r\bar{r} + b\bar{b}b\bar{b} + r\bar{b}r\bar{b} + b\bar{r}r\bar{b}\right)-\left(r\bar{r}r\bar{r} + b\bar{b}b\bar{b} + b\bar{r}r\bar{b} + r\bar{b}b\bar{r}\right)$$
$$+\left(r\bar{r}r\bar{r} + b\bar{b}b\bar{b} + b\bar{b}r\bar{r} + r\bar{r}b\bar{b}\right)] = \frac{1}{2}\left|F=2,F^3=2\right\rangle\otimes\left(\left|X_0^C\right\rangle + \sqrt{3}\left|X_E^C\right\rangle\right)$$

$\left|X_0^C\right\rangle, \left|X_E^C\right\rangle$ are the color singlet analogues of the flavor singlets defined in equation 2.7b.

After antisymmetrizing, there remain ten linearly independent 4-body states. The results of applying the antisymmetrizer, A, to all possible flavor and color combinations, are shown below in symbolic form.

$$A\left|F=2,F^3\right\rangle\otimes\left|C=0,C^3=0\right\rangle = \frac{1}{2}\left|F=2,F^3\right\rangle\otimes\left(\left|X_0\right\rangle + \sqrt{3}\left|X_E\right\rangle\right) \qquad (2.10a)$$

Note that the choice of color singlet eigenfunction is immaterial; using $\left|X_0^C\right\rangle$, $\left|X_E^C\right\rangle$ for $\left|C=0,C^3=0\right\rangle$ would give the same result. This observation also holds true for the triplet flavor states that have ts or st coupling.

$$A\left|F=1,F^3\right\rangle_{st,ts}\otimes\left|C=0,C^3=0\right\rangle =$$
$$\frac{1}{\sqrt{8}}\left(\left|F=1,F^3\right\rangle_{ts} + \left|F=1,F^3\right\rangle_{st}\otimes\left(\left|X_{0)}\right\rangle + \sqrt{3}\left|X_E\right\rangle\right)\right) \qquad (2.10b)$$

However, the antisymmetrizer extinguishes any triplet flavor state that has tt (triplet-triplet) coupling regardless of the color eigenstate used.

$$A\left|F=1,F^3\right\rangle_{tt}\otimes\left|C=0,C^3=0\right\rangle = 0$$

There are four remaining possibilities; two flavor singlets, and two color singlets give four possible combinations to consider. Only two of these combinations, however, give linearly independent outcomes summarized below.

$$\begin{aligned} &A\left|F=0,F^3=0\right\rangle_{tt}\otimes\left|C=0,C^3=0\right\rangle_{tt}= \\ &A\left|F=0,F^3=0\right\rangle_{ss}\otimes\left|C=0,C^3=0\right\rangle_{ss} \\ &=\frac{1}{\sqrt{8}}\left(\begin{array}{l}\left|F=0,F^3=0\right\rangle_{tt}\otimes\left[\left|X_0^C\right\rangle-\sqrt{3}\left|X_E^C\right\rangle\right] \\ +\left|F=0,F^3=0\right\rangle_{ss}\otimes\left[\sqrt{3}\left|X_0^C\right\rangle+\left|X_E^C\right\rangle\right]\end{array}\right) \end{aligned} \tag{2.10c}$$

Note that when the flavor and color couplings are both tt or both ss, the results are identical. The remaining two possibilities, coupling the flavor tt to the color ss, or flavor ss to color tt yields identical outcomes.

$$\begin{aligned} &A\left|F=0,F^3=0\right\rangle_{ss}\otimes\left|C=0,C^3=0\right\rangle_{tt}=A\left|F=0,F^3=0\right\rangle_{tt}\otimes\left|C=0,C^3=0\right\rangle_{ss}= \\ &\frac{1}{\sqrt{8}}\left(\left|F=0,F^3=0\right\rangle_{tt}\otimes\left[\left|X_E^C\right\rangle+\sqrt{3}\left|X_0^C\right\rangle\right]+\left|F=0,F^3=0\right\rangle_{ss}\otimes\left[\sqrt{3}\left|X_E^C\right\rangle-\left|X_0^C\right\rangle\right]\right) \end{aligned} \tag{2.10d}$$

The ten states we have formed thus far in 2.10a-d (5 quintuplet flavor states, 3 flavor triplet states, and 2 flavor singlet states coupled to color singlets) constitute an orthonormal set of eigenstates antisymmetric under exchange of identical particles. Before we embark on the next step and investigate a few interesting Hamiltonians in this toy model, we should reflect on the results of our efforts thus far.

We should note that $\left|X_0^C\right\rangle+\sqrt{3}\left|X_E^C\right\rangle$ is a color singlet state antisymmetric under exchange of identical particles. Any flavor state that is attached to this combination is symmetric (this is why the flavor triplet state that came from tt coupling vanished under the action of the antisymmetrizer, A).

The lessons learned are two-fold: first, color singlet eigenstates will mix under antisymmetrization and, although this is expected, it complicates the issue of identifying

what is meant by "exotic"; second, antisymmetrization by itself makes certain states impossible. (There were 32 possible states above, but only 10 survived antisymmetrization.)

Now that we have completed the construction of our orthonormal basis, we investigate the results of certain Hamiltonians in our model.

Model Hamiltonians in Flavor and Color Space

Any Hamiltonian proposed here could not be dynamical since only internal symmetries are affected in our model. A dynamical model would couple internal symmetries with external potentials such as the ones we investigate in later chapters. Since the states defined in the previous section have no spatial dependence, we are restricted to using combinations of SU(2) group generators (flavor and /or color) to build a reasonable interaction.

Two candidate interactions will be proposed and their symmetries will be investigated to illuminate the action of these Hamiltonians on the group structure of the flavor and color wavefunctions. We shall start with the simplest, a Hamiltonian which is simply a product of the color and flavor analogues of equation 2.3.

$$H_1 = \sum_{i,j} \vec{F}_i \bullet \vec{F}_j \sum_{k,m} \vec{\lambda}_k \bullet \vec{\lambda}_m \tag{2.11}$$

Again, we have i and j, k and m, as particle labels and $\vec{F}$ is the flavor analogue of $\vec{\lambda}$ in color space. It should be apparent that equation 2.11 represents a very simple interaction; indeed, using 2.3, we can see that 2.11 can be rewritten as follows.

$$H_1 = \frac{1}{4}\left(\vec{\lambda}^2 - \sum_i \vec{\lambda}_i^2\right)\left(\vec{F}^2 - \sum \vec{F}_i^2\right) \tag{2.11a}$$

This form clearly shows that H_1 will preserve full flavor and color symmetry since it is simply a function of the respective Casimir operators in color and flavor space. This means that 2.11a will conserve $\vec{F}^2, F^3, \vec{\lambda}^2, \lambda^3$ a maximum set of symmetries. This Hamiltonian would not mix any of the states defined in 2.10a-d.

A more interesting Hamiltonian, given in equation 2.12, exhibits the same symmetries as 2.11 (although this is not obvious) but raises the possibility of some mixing.

$$H_2 = \sum \vec{F}_i \bullet \vec{F}_j \vec{\lambda}_i \bullet \vec{\lambda}_j \tag{2.12}$$

The main difference from 2.11 lies in the fact that both the flavor and color operators are acting on the same pair of particles simultaneously; in 2.11 the sums over the flavor and color interactions were separable, but in 2.12 they are not. It is possible to show that H_2 is diagonal in the basis defined in equations 2.10a-d. The eigenvalues of the flavor singlets in 2.10c and 2.10d are the 3/8 and –3/8, respectively, and raises the possibility that they may dynamically be different in a model space that includes spatial interactions.

We will now show that H_2 possesses the same symmetries as H_1. It is only necessary to show that H_2 commutes with $\vec{F}^2, F^3$. Since both color and flavor obey SU(2) relations, the case for the color operators would be redundant.

Recall the commutation relations for the group generators of SU(2).

$$\left[F^a, F^b\right]_- = i\varepsilon^{abc} F^c \tag{2.13}$$

$$\varepsilon^{abc} = \begin{cases} 1, \text{even} \\ -1, \text{odd} \\ 0, \text{identical} \end{cases}$$

Even, odd and identical refer, respectively, to an even (or cyclic) permutation of indices, an odd permutation of indices, and the case where any of the indices are identical. This

background allows us to discover the symmetries of our Hamiltonian. First, it shall be proven that H_2 commutes with F^3. In what follows liberal use shall be made of the identities:

$$\begin{aligned}[AB,C] &= A[B,C]+[A,C]B \\ [A,BC] &= B[A,C]+[A,B]C\end{aligned} \tag{2.15}$$

It is sufficient to examine one term in the Hamiltonian; all other terms are exactly similar and amount to permutations of indices. We choose the following term.

$$\left[\vec{\lambda}_1 \bullet \vec{\lambda}_3 \vec{F}_1 \bullet \vec{F}_3, F_1^3 + F_2^3 + F_3^3 + F_4^3\right] = \vec{\lambda}_1 \bullet \vec{\lambda}_3 \left[\vec{F}_1 \bullet \vec{F}_3, F^3\right] \tag{2.16}$$

This follows by 2.15 and the fact that color operators commute with flavor operators. Also, we know that all operators with different particle labels commute. This allows us to consider fewer terms in 2.16 when we expand the dot products.

$$\left[F_1^1 F_2^1 + F_1^2 F_2^2, F_1^3 + F_2^3\right] = F_2^1\left[F_1^1, F_1^3\right] + F_2^2\left[F_1^2, F_1^3\right] + F_1^1\left[F_2^1, F_2^3\right] + F_1^2\left[F_2^2, F_2^3\right] =$$
$$-iF_2^1 F_1^2 + iF_2^2 F_1^1 - iF_1^1 F_2^2 + iF_1^2 F_2^1 = 0$$

This result implies that $\left[H_2, F^3\right] = 0$, as advertised. Now we turn to the Casimir operator of SU(2) flavor. Again it suffices to consider a single term in the Hamiltonian as before:

$$\left[\vec{\lambda}_1 \bullet \vec{\lambda}_3 \vec{F}_1 \bullet \vec{F}_3, \vec{F}^2\right] = \vec{\lambda}_1 \bullet \vec{\lambda}_3 \left[\vec{F}_1 \bullet \vec{F}_3, \sum_i \vec{F}_i^2 + 2\sum_{i<j} \vec{F}_i \bullet \vec{F}_j\right] \tag{2.17}$$

Since the single particle Casimir operators in the first sum in the commutator in 2.17 commutes with all terms, and keeping in mind that operators with different particle labels commute, we only need consider a relatively small number of factors, namely these:

$$\begin{aligned}&\left[\vec{F}_1\bullet\vec{F}_3,\vec{F}_1\bullet\vec{F}_2+\vec{F}_2\bullet\vec{F}_3\right]+\left[\vec{F}_1\bullet\vec{F}_3,\vec{F}_1\bullet\vec{F}_4+\vec{F}_3\bullet\vec{F}_4\right]=\\&i\left(F_3^1F_2^2F_1^3-F_3^1F_2^3F_1^2-F_3^2F_2^1F_1^3+F_3^2F_2^3F_1^1+F_3^3F_2^1F_1^2-F_3^3F_2^2F_1^1\right)+\\&i\left(-F_1^2F_2^1F_3^3+F_1^2F_2^3F_3^1+F_1^1F_2^2F_3^3-F_1^1F_2^3F_3^2+F_1^3F_2^1F_3^2-F_1^3F_2^2F_3^1\right)=0\end{aligned}\qquad(2.17a)$$

Hence, this more complicated Hamiltonian preserves the same symmetries as the one defined in equation 2.11. A further consequence of what has been done so far is that $[H_1,H_2]=0$ although this will not be shown explicitly.

Summary and Conclusions

The background of this chapter and the preceding analysis of our toy model suggest that many of the questions raised in the Introduction await complete answers only in the context of a fully dynamical model. We are in a position, however, to state certain expectations of that future model based on the considerations and analysis of this chapter. It happens that modeling color with SU(2) instead of SU(3) is adequate for answering some questions. Like SU(2), the color group SU(3) also has two singlets in the 4-body problem we have examined here; indeed, there exists a linear combination of these SU(3) singlets which is antisymmetric just like the color SU(2) model. Hence the states we found in 2.10a-d should be closely emulated in an SU(3) model.

There are differences, however, but they pose no real obstacle. For example, it is well-known that it is not possible to find an SU(3) antitriplet that transforms the same way as the particle triplet does. We saw in SU(2) that it was possible to find an antidoublet that transformed as the particle doublet does (cf. equation 2.6). This can be traced to the fact that SU(3) has two diagonal generators versus only one diagonal generator in SU(2). This does not really affect the results of this chapter; the only practical impact is that the coupling of SU(3) states is more complicated than SU(2) and requires the use of isoscalar factors [9,10] in addition to the ordinary Clebsch-Gordon coupling.

These reflections lead us to state the main conclusions of this chapter. If we take H_1 or H_2 as an operator that may multiply some dynamical interaction term, it may be

possible to break flavor symmetry. As we have noted, different flavors of quark have different electrical charges. This could lead to a charge symmetry breaking that mixes states of different flavor. A Coulomb interaction may be tailor-made for this. The electroweak interactions are known to break this symmetry [4], but this question will not be addressed in this thesis.

References

[1] H. Georgi, *Lie Algebras in Particle Physics*, (Addison-Wesley, Reading, 1982).

[2] Wu-Ki Tung, *Group Theory in Physics*, (World Scientific Publishing Company, Philadelphia, 1985).

[3] M. E. Peskin and D. V. Schroeder, *An Introduction to Quantum Field Theory,* (Addison-Wesley Publishing Company, Reading, Massachusetts, 1995).

[4] F. Halzen and A. D. Martin, *Quarks & Leptons: An Introductory Course in Modern Particle Physics*, (John Wiley & Sons, New York, 1984).

[5] M. E. Rose, *Elementary Theory of Angular Momentum*, (Dover Publications, Inc., New York, 1957).

[6] H. A. Bethe and R. Jackiw, *Intermediate Quantum Mechanics*, (Addison-Wesley, Reading, Massachusetts, 1997). 3rd ed.

[7] W. Greiner and B. Mueller, *Quantum Mechanics: Symmetries* (Springer-Verlag, New York, 1994), 2nd ed.

[8] D. Griffiths, *Introduction to Elementary Particles,* (John Wiley & Sons, Inc., New York, 1987).

[9] J. J. de Swart, Rev. Mod. Phys. **35**, 916 (1963).

[10] P. McNamee and F. Chilton, Rev. Mod. Phys. **36**, 1005 (1964).

3 FOUNDATIONS OF MANY FERMION DYNAMICS (MFD)

Introduction

In this chapter we will introduce the formal components needed to build a computational scheme that will be applied to many-fermion systems. This computational scheme is designated as Many-Fermion Dynamics (MFD) [1].

MFD, at present, is developed to treat systems in two types of specialized applications. The first application addresses many body problems in the bound (and quasi-bound) states of nuclei and other systems where color and flavor degrees of freedom are not involved. This framework is referred to as MFDn. The second application, developed within this project, is tailored to treat fermionic systems with color and flavor symmetries included and is designated MFDq.

Both versions have many features in common. Here we provide an overview of these features with a summary of the main differences. First, they employ the same spatial component of the single particle basis to construct many-body states, the simple harmonic oscillator (SHO) basis. Second, they both employ spin ½ single particle states and this is a very simple feature to change. Third, both frameworks may treat problems with two species of fermions. Class 1 (Class 2) particles are protons (neutrons) in MFDn and quarks (antiquarks) in MFDq. The fact that MFDq incorporates antiparticles introduces complications in the SU(2) flavor coupling treated in Chapter 2 that are not treated in MFDn. Fourth, once the single particle basis is enumerated for either one or two classes of fermions, MFDn and MFDq enumerate the many-body basis states in the m-scheme subject to constraints specified as data by the user. By the "m-scheme" we mean that many-body basis states are formed from unique sets of single particle states that each specify all available quantum numbers of a single particle, including its magnetic projection, m, of the

total angular momentum, J. Fifth, the many-body Hamiltonian is evaluated in the many-body basis space. At this point MFDn and MFDq employ very different techniques, as MFDn requires input of antisymmetrized and coupled 2-body (or 3-body) matrix elements of the fundamental Hamiltonian. On the other hand, MFDq requires input of product space 2-body matrix elements computed in the space, spin and isospin spaces. MFDq then forms antisymmetric 2-body matrix elements by treating the color, flavor and attendant particle-antiparticle degrees of freedom explicitly and computes the color factors necessary for each interaction in the fundamental Hamiltonian. Sixth, once the many-body Hamiltonian is evaluated, both MFDn and MFDq carry through a Lanczos iterative diagonalization process. Seventh, the resulting eigenvectors and eigenvalues are transformed from the Lanczos dynamical basis back to the original many-body basis. Finally, various observables are evaluated with the converged eigenvectors.

In the rest of this chapter we will proceed sequentially, discussing detailed features of MFD that are common to both MFDn and MFDq. We will then further elucidate the aspects that are specialized for each approach.

The Simple Harmonic Oscillator

In our study of many-body systems it is necessary to choose a single particle basis from which to build a many body basis. The SHO provides such a single particle basis that has many advantages; its properties are well known and it has been applied to nuclear shell model problems and other systems with success [2,3]. The SHO basis states are the exact single particle eigenstates of the following problem in Schroedinger wave mechanics.

$$\left(-\frac{\hbar^2}{2M}\nabla^2+\frac{1}{2}M\Omega^2 r^2\right)\Psi(r,\theta,\varphi)=E\Psi(r,\theta,\varphi) \tag{3.1}$$

The solution to this eigenvalue equation is given in many standard references [5,7].

$$\Psi(r,\theta,\theta) = R_{nl}(r)Y_{lm}(\theta,\varphi)$$
$$R_{nl}(r) = \sqrt{\frac{2(2v)^{l+3/2}\,n!}{[\Gamma(n+l+3/2)]^3}}\, r^{l+1} e^{-vr^2} L_{n+l+1/2}^{l+1/2}(2vr^2) \qquad (3.1a)$$
$$v = M\Omega / 2\hbar$$
$$E_{nl} = (2n+l+3/2)\hbar\Omega$$

$L_{n+l+1/2}^{l+1/l}$ are the associated Laguerre functions, and Y_{lm} are the spherical harmonic functions[7]. This solution constitutes the basis for the spatial wavefunctions that we will need. To incorporate spin we take a simple tensor product of the functions in equation 3.1 with the SU(2) spinor defined in Chapter 2. Strong isospin, another SU(2) symmetry commonly found in nuclear problems, may be included similarly. Many-body states are then constructed for use in the schemes of MFDn or MFDq. Pedagogically, we shall discuss 2-body states used by MFDn first since MFDq is a specialized adaptation of the nucleon treatment adopted in MFDn.

The Basics of 2-body States in MFDn

We wish to present a general formalism in 2nd quantized notation to simplify understanding of the essential features of 2-body states and their matrix elements. We shall then specialize to an explicit representation of 2-body matrix elements in the SHO basis. We start by specifying the anti-commutation relations of the creation and annihilation operators for identical fermions.

$$[a_i^+, a_j]_+ \equiv a_i^+ a_j + a_j a_i^+ = \delta_{ij} \qquad (3.2)$$

The following specifies the action of these operators on the vacuum.

$$\begin{aligned} a_i^+|0\rangle &= |i\rangle \\ a_i|0\rangle &= 0 \end{aligned} \tag{3.3}$$

We may define a many body antisymmetric state of single particle states (Slater determinant) that are eigenstates of some general, unperturbed Hamiltonian as follows.

$$\begin{aligned} \left(a_i^+ a_j^+ ... a_n^+\right)_\alpha |0\rangle &= |\varphi_\alpha\rangle \\ H_0|\varphi_\alpha\rangle &= E_\alpha|\varphi_\alpha\rangle \\ E_\alpha &= e_i + e_j + ... + e_n \end{aligned} \tag{3.4}$$

The e_i are single particle energies and each subscript i, j,…,n denotes a set of quantum numbers that describe the single particle state $\{n, l, s, j, m_j, \tau, \tau_z\}$ for nucleons and $\{n, l, s, j, m_j, \tau, \tau_z, I_z, Y, B\}$ for quarks. The global subscript α represents a unique set of values for the subscripts i,j,…,n and hence α is a shorthand index for our many-body basis states.

If we take the 2-body version of 3.4, and then couple those 2-body states to total angular momentum, J, and total strong isospin, T, we denote the states as $|abJT\rangle$. The symbols "a" and "b" represent a subset of the single particle quantum numbers, $\{n, l, s, j, \tau\}$ for nucleons and $\{n, l, s, j, \tau, I_z, Y, B\}$ for quarks, in the 2-body state. Antisymmetrization can be made explicit by referring to a direct product space that is designated by commas separating the single particle state labels.

$$|abJT\rangle = \frac{1}{\sqrt{2}}\left[|a, bJT\rangle - |b, aJT\rangle\right] \tag{3.5}$$

The state $|a, bJT\rangle$ is simply a product state coupled to good J and T. For nucleons, one may verify that the antisymmetric state for a=b vanishes unless J+T=odd. Matrix elements of a

general operator, R, in the antisymmetrized 2-body SHO basis of 3.5 are calculated by the following relationship [5]. For identical particles the phase relations of the 9-j symbols

$$\langle abJT|\hat{R}|cdJT\rangle = \frac{1}{\sqrt{(1+\delta_{ab})(1+\delta_{cd})}} \sum_{n\ln' l' \Im N\ell} \left[1-(-1)^{l+S+T}\right] \langle nl|\hat{R}^{\Im ST}|n'l'\rangle$$

$$* \left\{ \sum_{L} (-1)^{L} (2L+1) \sqrt{(2\Im+1)(2S+1)(2j_a+1)(2j_b+1)}\, W(\ell lJS;L\Im) \right\}$$

$$* \left\{ \begin{Bmatrix} l_a 1/2 j_a \\ l_b 1/2 j_b \\ L \;\; S \;\; J \end{Bmatrix} \langle nlN\ell \| n_a l_a n_b l_b L\rangle \right\} \tag{3.6}$$

$$* \left\{ \sum_{L'} a \to c, b \to d, L \to L', n \to n', l \to l' \right\}$$

and the oscillator brackets $\langle \mathrm{nlN}\ell, \mathrm{L} \| \mathrm{n_1 l_1 n_2 l_2}, \mathrm{L} \rangle$ under particle exchange are extremely important. The W( ) symbols are the Racah coefficients which are related to the 6-j symbols [6]. First we shall deal with the phase relationships of the 9-j symbols. We should note that the center of mass oscillator quantum numbers in 3.6 are N and ℓ while the relative quantum numbers are n, l, and their primed counterparts.

$$\begin{Bmatrix} l_a 1/2 j_a \\ l_b 1/2 j_b \\ L \;\; S \;\; J \end{Bmatrix} = (-1)^{\Delta} \begin{Bmatrix} l_b 1/2 j_b \\ l_a 1/2 j_a \\ L \;\; S \;\; J \end{Bmatrix} \tag{3.7}$$

$$\Delta = l_a + l_b + 1/2 + 1/2 + j_a + j_b + L + S + \mathrm{J}$$

The phase relationships of the 9-j symbols are shown above in 3.7.

We investigate the phase relationship of the oscillator brackets which bear a specific connection to the Brody-Moshinsky bracket, M_L, [4] introduced below. We then deduce

the oscillator bracket phases from the phase relations of the Moshinsky bracket for an interchange of identical particles.

$$\begin{aligned} &M_L(n_1l_1n_2l_2;N\ell nl)=(-1)^{\ell-L}M_L(n_2l_2n_1l_1;N\ell nl) \\ &\langle nlN\ell,L\|n_1l_1n_2l_2,L\rangle=(-1)^{\ell+l-L}M_L(n_1l_1n_2l_2;N\ell nl)=(-1)^{\ell-L}\langle nlN\ell\|n_2l_2n_1l_1,L\rangle \end{aligned} \tag{3.8}$$

We use the fact that parity is conserved, which implies that 3.8a is true. This allows

$$(-1)^{\ell+l}=(-1)^{l_1+l_2} \tag{3.8a}$$

us to see that the net phase of a bra or ket under interchange, using 3.7, 3.8 and 3.8a, is given

$$\begin{aligned} &(-1)^{L+S+\ell-L+\beta}=(-1)^{S+\ell+\beta}=(-1)^{l_1+l_2+l+S+\beta}=(-1)^{l_1+l_2+1-T+\beta} \\ &\beta=J+1+j_a+j_b \end{aligned} \tag{3.9}$$

by 3.9, where we have used the fact that terms in the outer sum of 3.6 with $1+S+T$ =even gives a zero contribution. This restriction is the practical implementation of 3.5 that forces the wavefunction to be antisymmetric in nucleon applications.

After these matrix elements are constructed, they serve as inputs to MFDn to build the many-body Hamiltonian. Then a Lanczos method is employed to diagonalize the Hamiltonian for the many body problems in (primarily) nuclear physics applications. The Lanczos method shall be outlined later, but we shall first introduce the treatment of 2-body states in MFDq.

The Basics of 2-body States in MFDq

In contrast to MFDn, which uses antisymmetrized 2-body matrix elements as inputs, MFDq utilizes product space matrix elements coupled to good total angular momentum, J

and total isospin, T (T is adapted for use as a flavor quantum number, F, in MFDq as per Chapter 2). SU(3) color labels Y and I^3 are attached to the product space wavefunctions $|a,bJT\rangle$ where a,b now refer to the reduced quantum numbers of the single particle states for the quark applications as defined previously. The 2-body matrix elements that serve as inputs to MFDq are constructed by modifying 3.6. Specifically, the factors that enforce antisymmetry for nucleons are removed and we work directly in the product space. The result follows here for color-blind operators acting on relative coordinates.

$$\langle a,bJT|\hat{R}|c,dJT\rangle = \sum_{nln'l'S\Im} \langle nl|\hat{R}^{\Im ST}|n'l'\rangle$$

$$*\left\{\sum_{L}(-1)^{L}(2L+1)\sqrt{(2\Im+1)(2S+1)(2j_a+1)(2j_b+1)}W(\ell lJS;L\Im)\right.$$

$$\left.*\begin{Bmatrix} l_a 1/2 j_a \\ l_b 1/2 j_b \\ L \;\; S \;\; J \end{Bmatrix}\langle nlN\ell \| n_a l_a n_b l_b L\rangle\right\} \qquad (3.10)$$

$$*\left\{\sum\; a\to c, b\to d, L\to L', n\to n', l\to l'\right\}$$

The phase relations in 3.8 and 3.8a are retained, but the specialized result in 3.9 is discarded since quark product states do not obey the $l+S+T$ =odd rule. Instead, we now evaluate and store pairs of matrix elements $\langle a,bJT|\hat{R}|c,dJT\rangle$ and $\langle a,bJT|\hat{R}|d,cJT\rangle$ for later coupling with color and flavor degrees of freedom within MFDq. The product space 2-body matrix elements serve as input to MFDq which then implements multiplication by color matrix elements in the product space. Antisymmetrization proceeds directly via 3.5 for quark-quark (or antiquark-antiquark) 2-body matrix elements. The simple product form is retained as in 3.10 for quark-antiquark matrix elements since antisymmetry is not required by the Pauli principle under exchange of particle and antiparticle. For operators with color

dependence, the assumed form in the product space is given by equation 2.3. The matrix elements of the color operator simply multiply 3.10.

Now that the critical inputs to MFD are at hand, we shall outline the main algorithm MFD uses to compute the spectrum of the Hamiltonian and obtain the associated eigenvectors. The FORTRAN code of the Hamiltonian subroutine of MFDq is included as an Appendix in order to show the practical implementation of these features.

The Lanczos Method

The Lanczos method is an iterative procedure that attempts to obtain the eigenvalues and eigenvectors of a model Hamiltonian. The basic algorithm [8,9] requires a trial vector, $|\chi_1\rangle$ (with $b_0 = 0$) to begin the iteration, which is outlined below. The "$\pm$" appearing in the Lanczos algorithm is simply a reflection of the overall phase uncertainty that any quantum state possesses. In our implementation, we adopt the convention of taking the positive square root. Of course, this has no consequences for any observable quantity.

$$
\begin{aligned}
|\eta_{n+1}\rangle &= H|\chi_n\rangle - b_n|\chi_{n-1}\rangle \\
a_n &= \langle\eta_{n+1}|\chi_n\rangle \\
|\eta'_{n+1}\rangle &= |\eta_{n+1}\rangle - a_n|\chi_n\rangle \\
b_{n+1} &= \pm\left[\langle\eta'_{n+1}|\eta'_{n+1}\rangle\right]^{1/2} \\
|\chi_{n+1}\rangle &= \frac{|\eta'_{n+1}\rangle}{b_{n+1}}
\end{aligned}
$$

This algorithm produces a tri-diagonal Hamiltonian matrix that is unitarily equivalent [8] to the original matrix and can be diagonalized far more efficiently than many brute force methods when we seek systematic convergence to the lowest eigenvalues and eigenvectors. Lanczos performs best on large, sparse matrices that exhibit little or no degeneracy in their spectrum, and converges to a stable result very quickly in these cases. There is some sensitivity to the choice of the initial trial vector, and Lanczos does not

always preserve orthogonality of the eigenstates. Hence, care must be taken to re-orthogonalize after each iteration [8].

The CM Projection Method

When the spectrum of the chosen Hamiltonian is computed, the associated eigenstates may have undesirable mixtures of CM motion. When mixtures of CM motion are present, the relative motion component becomes a mixture of relative motion eigenstates. Hence, the properties of states with mixtures of CM excitations should not directly be compared to experimental data. Since our Hamiltonians are translationally invariant, i.e. the kinetic energy and interactions are functions only of relative coordinates, we demand solutions with a pure state of CM motion that can be easily factored out of all observables. It is necessary, then, to discard states with excited CM motion and retain states that have relative motion and a pure CM wavefunction only. A method for accomplishing this is outlined below. As before we will start with a 2-body example and then generalize to an A-body framework.

Suppose we have a Hamiltonian of the following form that describes the interaction of two particles of the same mass. Then we may define the CM and relative coordinates and

$$H = \frac{\vec{p}_1^{\,2}}{2m} + \frac{\vec{p}_2^{\,2}}{2m} + V\left(\left|\vec{r}_1 - \vec{r}_2\right|\right)$$

$$\vec{R} = \left(\frac{\vec{r}_1 + \vec{r}_2}{2}\right)$$

$$\vec{r} = \vec{r}_1 - \vec{r}_2$$

$$\vec{P} = \vec{p}_1 + \vec{p}_2$$

$$\vec{p} = \frac{1}{2}\left(\vec{p}_1 - \vec{p}_2\right)$$

$$\Rightarrow H = \frac{\vec{P}^2}{2M} + \frac{\vec{p}^{\,2}}{2\mu} + V(\vec{r})$$

momenta in a way that allows the Hamiltonian to be written in a separable form as shown above. We define M=2m and μ=m/2. The first term in the transformed Hamiltonian above describes the free motion of the CM of the 2-body system and the remaining terms describe a 1-body problem for a particle interacting via potentials expressed in relative coordinates. We now employ this insight to rid ourselves of the unphysical CM motion mentioned earlier for the case of A particles with identical masses interacting via a potential that involves only relative coordinates. The straightforward generalization of the CM kinetic energy (and CM

$$\begin{aligned} T_{cm} &\equiv \frac{\vec{P}^2}{2M} = \frac{1}{2M}\left(\sum_i \vec{p}_i\right)^2 \\ U_{cm} &= \frac{1}{2}M\Omega^2\left[\frac{1}{A}\sum_i \vec{r}_i\right]^2 \\ M &= Am \end{aligned} \tag{3.11}$$

oscillator potential) is quite simple. If we now define H_{cm} as the sum of both terms in 3.11, we now have an operator capable of acting on the CM coordinates with eigenvalues as given in 3.1a. This allows a clear and easy identification of CM excited states. Hence our full Hamiltonian may be written as follows. (The interaction V_{rel} is usually a 2-body operator.)

$$H = T_{rel} + V_{rel} + \alpha\left(H_{cm} - \frac{3}{2}\hbar\Omega\right)$$

The constant factor of 3/2 $\hbar\Omega$ is subtracted in MFD so that the spectra of states with no CM motion will not have zero point energy. The constant α is taken sufficiently large so that CM excited states lie above all of the physical states obtained by the Lanczos method. Examples of this will be demonstrated in Chapter 4.

Summary and Conclusions

The development in this chapter has provided a basis for computing the spectrum of a given Hamiltonian in the SHO basis for an arbitrary number of fermions. Although MFDn and MFDq are specially modified to address nuclear and sub-nuclear quark applications, the formalism in this chapter is general enough to be adapted for a variety of uses.

References

[1] J. P. Vary, *The Many-Fermion Dynamics Shell-Model Code*, Iowa State University (1992, unpublished); J. P. Vary and D. C. Zheng, *ibid.*, (1994, unpublished).

[2] P. Navratil, J. P. Vary, and B. R. Barrett, Phys. Rev. C **62,** 054311 (2000)

[3] P. Navratil, J. P. Vary and B. R. Barrett, Phys. Rev. Lett. **84**, 5728 (2000)

[4] T. T. Kuo and G. E. Brown, Nucl. Phys. **85** (1966) 40.

[5] A. de-Shalit and I. Talmi, *Nuclear Shell Theory*, (Academic Press, New York, 1963).

[6] M. E. Rose, *Elementary Theory of Angular Momentum*, (Dover Publications, New York, 1957).

[7] G. Arfken, *Mathematical Methods for Physicists*, (Academic Press, New York, 1985), 3rd ed.

[8] B. N. Parlett, *The Symmetric Eigenvalue Problem*, (Prentice-Hall, Englewood Cliffs, 1980).

[9] R. A. Willoughby, *Lanczos Algorithms for Large Symmetric Eigenvalue Computations Volume I: Theory*, (Society for Industrial &Applied Mathematics, Portland, 2002) 1st ed.

4 TESTING MFD

Introduction

In this chapter we investigate the two schemes for many-fermion systems introduced in Chapter 3, MFDq and MFDn. The first section of this chapter shows the results of comparison tests between MFDn and MFDq for a series of 2-body problems. A later section deals with self-consistency checks of MFDq itself on 4-body problems and basis spaces of that will be detailed as the need arises.

To reiterate and summarize the differences between these frameworks, we will note that MFDn treats all particles (neutrons and protons, generically) as colorless with the option of selecting an SU(2) strong isospin symmetry that is adapted in MFDq for an SU(2) flavor treatment of all particles. MFDq also implements a full treatment of SU(3) color symmetry. We must also involve antiparticles in our consideration, and this fact complicates the treatment as outlined in Chapter 2, i.e. there are separate flavor doublets for particle and antiparticle in MFDq whereas MFDn allows only a particle doublet of strong isospin. We do not, however, explore isospin symmetry breaking (accessible in MFDn), nor do we examine flavor symmetry breaking (accessible in MFDq) in the present investigation.

Both MFDn and MFDq allow inclusion of two classes of fermions in our calculations; the proton (neutron) in class 1 (class 2) in MFDn is the analog of the quark (antiquark) in MFDq. These differences grant MFDn only a limited ability to emulate many-body quark systems treated in MFDq and force us to examine $q\bar{q}$ as the only (almost exactly) analogous system in both schemes. We will later test MFDq on a set of 4-body calculations selected to check for a proper treatment of all possible matrix elements in the many-body problem.

Systematic Test Comparison of MFDn and MFDq in the 2-Body Problem

A procedure was adopted that introduced terms in our model Hamiltonian sequentially. This provided for a careful, complete comparison of MFDn and MFDq that allowed us to deduce the quantum number content of many states and perform consistency analyses on the spectra. In what follows in this section, we restrict our basis space to a "$2\hbar\Omega$" calculation. Our basis space definitions follow Ref. [1]. This means that for a "$2\hbar\Omega$" basis space, the maximum number of allowed excitations in our simple harmonic oscillator basis (SHO) is limited by the restriction that the sum over the oscillator quanta of all particles is less than or equal to 2 (cf. equation 3.1).

In our first comparison, the eigenvalues of the Hamiltonian and their degeneracy for the non-relativistic relative kinetic energy operator are recorded in Table 4.1.

Table 4.1: A systematic comparison of eigenvalues (in MeV) from MFDq and MFDn for case 1. Multiplicity is given in square brackets.

MFDn[a]	MFDq
112.5 [3]	112.5 [18]
187.5 [4]	187.5 [24]
262.5 [3]	262.5 [18]

[a] An oscillator spacing of $\hbar\Omega$ =150 MeV and a constituent quark mass, m_q =330 MeV, was was used in these calculations. The magnetic projection of the total angular momentum was restricted to M=2. 100 Lanczos iterations were used to obtain these results.

The relative multiplicity of the eigenvalues from MFDn and MFDq is due to the extra quantum numbers incorporated into MFDq. The factor of 6 can be easily explained by reference to color and flavor quantum numbers. Flavor is an SU(2) symmetry in our investigation and we have required $\sum_i F_i^3 = 0$ where F^3 is the third component of flavor and i is a particle label. (In MFDn we have required $\sum_i T_i^3 = 0$ where T^3 is the third component of strong isospin.) For two particles, there is a flavor singlet and one state in the flavor triplet

that satisfies this requirement and this fact gives rise to a relative multiplicity of 2. Color is an SU(3) symmetry and has two quantum numbers upon which MFDq places restrictions. MFDq retains many-body fermion states only if they obey the "total color charge rule" defined by equation 2.4. For $q\bar{q}$ there is one color singlet and two states in the color octet configuration that match these criteria and gives a multiplicity of 3. Coupled with the consideration of flavor, the relative multiplicity of 6 is therefore easily understood.

In the next test considered, designated "case 2" we will see the degeneracy due to color lifted as we add a term to the Hamiltonian to separate the color singlet states from the non-singlet states. The flavor degeneracy will not be lifted since the model Hamiltonians we will use are not flavor sensitive.

Table 4.2: A systematic comparison of eigenvalues (in MeV) from MFDq and MFDn for case 2. Multiplicity is given in square brackets.

MFDn [a]	MFDq
112.5 [3]	112.5 [6]
187.5 [4]	187.5 [8]
262.5 [3]	262.5 [6]

[a] Here $H = T_{rel}$ in the case of MFDn. $H = T_{rel} + \kappa\vec{\lambda}\bullet\vec{\lambda}$ and $\kappa = 7000$ MeV for MFDq.

Note that the eigenvalues are unchanged, but the relative multiplicity of the physical states between MFDn and MFDq has fallen to 2 which indicates that only the color singlet states have been retained in the low-lying spectrum. A sufficiently large value of κ was chosen to achieve good separation between the physical color singlet states and the unphysical non-singlet states that are now several GeV higher in the spectrum than the singlet states.

The physical states can be decomposed into a product of a wavefunction that describes the intrinsic motion (relative wavefunction) and a pure 0S harmonic oscillator wavefunction that describes the center of mass (CM) motion. For our next comparison we add to the Hamiltonian defined in Table 4.2 a harmonic oscillator operator,

$H_{cm} = T_{cm} + U_{cm}$ multiplied by a positive constant α, that acts only on the CM coordinates. H_{cm} is used to separate the spectrum of the physical states from the states with spurious CM motion. This is necessary since spurious CM motion does not contribute to the mass or other physical properties of the eigenstate. In other words the wavefunction of the physical states can be written as follows:

$$|\Psi\rangle = |nL, M\rangle_{rel} \otimes |0S, M' = 0\rangle_{cm}$$

An unphysical state would have the wavefunction $|\Psi\rangle = |nl, M\rangle_{rel} \otimes |n'L', M'\rangle_{cm}$ where $n'L' \neq 0S$, or $M' \neq 0$, or both. We note that n is the principal quantum number for the oscillator, $l(L')$ is the relative orbital angular momentum, and $M(M')$ is the magnetic projection of the total angular momentum, J, in the relative (CM) system. This means that $M_{tot} = M + M'$.

The states without CM motion will have the largest range of internal motions allowed in our basis space, and these are the physical states we seek. The states of excited CM motion, however, are essentially redundant copies of the physical states that are easily identified by the effects of αH_{cm} and a suitable choice of α allows for a straightforward classification of these excited CM states.

When case 2 and case 3 results are compared, it is apparent that the two lowest sets of degenerate eigenvalues of case 2 correspond to states with spurious center of mass motion.

Table 4.3: A systematic comparison of eigenvalues (in MeV) from MFDq and MFDn for case 3. Multiplicity is given in square brackets.

MFDn [a]	MFDq
262.5 [3]	262.5 [6]
1687.5 [4]	1687.5 [8]
3112.5 [3]	3112.5 [6]

[a] Here H = Trel + αH_{cm}, and α=10. $\kappa\vec{\lambda} \bullet \vec{\lambda}$ with κ=7000 MeV is added for MFDq.

Explicitly, we shall see that the first eigenvalue in Table 4.2 must belong to a state with the following decomposition: $|\Psi_1\rangle = |0S, M = 0\rangle_{rel} \otimes |0D, M' = 2\rangle_{cm}$. We employ the virial theorem to compute the lowest expected eigenvalue of T_{rel}, keeping in mind that T_{rel} acts only on the relative wavefunction:

$$\langle\Psi_1|\hat{T}_{rel}|\Psi_1\rangle = \frac{1}{2}\langle\Psi_1|\hat{T}_{rel} + \hat{U}_{rel}|\Psi_1\rangle = \frac{1}{2}(2n_{rel} + l_{rel} + \frac{3}{2})\hbar\Omega$$

$\hat{U}_{rel}$ is a relative harmonic oscillator potential. The states with the lowest energy due to relative motion have $2n_{rel} + l_{rel} = 0$ with $M_{rel} = 0$ and that gives an eigenvalue of $3/4\,\hbar\Omega$ =3/4*150 MeV=112.5 MeV. The eigenstate belonging to the second eigenvalue in Table 4.2 decomposes as $|\Psi_2\rangle = |0P, M = 1\rangle_{rel} \otimes |0P, M' = 1\rangle_{cm}$. Again we employ the virial theorem to compute the eigenvalue.

$$\langle\Psi_2|\hat{T}\,rel|\Psi_2\rangle = \frac{1}{2}\langle\Psi_2|\hat{T}\,rel + \hat{U}\,rel|\Psi_2\rangle = \frac{1}{2}(2n_{rel} + l_{rel} + \frac{3}{2})\hbar\Omega$$

With $2n_{rel} + l_{rel} = 1$, and $M_{rel} = 1$, we have $\frac{1}{2}(2n_{rel} + l_{rel} + \frac{3}{2})\hbar\Omega = \frac{5}{4}\hbar\Omega = 187.5$ MeV, the first excited state in this basis. Thus it follows that the two lowest sets of eigenvalues in Table 4.2 were due to spurious center of mass motion. Furthermore, the eigenvalues of 1687.5 and 3112.5 MeV in Table 4.3 are exactly10 $\hbar\Omega$ added to the middle eigenvalue and $20\hbar\Omega$ added to the lowest eigenvalue in Table 4.2, respectively. ($3/2\,\hbar\Omega$ is subtracted from αH_{cm} and thus yields an eigenvalue of $\alpha(2n_{cm} + l_{cm})\hbar\Omega$.) If we recall that αH_{cm} acts only on the center of mass wavefunctions in $|\Psi_1\rangle$ and $|\Psi_2\rangle$, we get eigenvalues of $\alpha\hbar\Omega$ for $|\Psi_2\rangle$ and $2\alpha\hbar\Omega$ for $|\Psi_1\rangle$, which adds 1500 MeV and 3000 MeV to the eigenvalues in

Table 4.2, reproducing the eigenvalues of 1687.5 and 3112.5 MeV in Table 4.3. This verifies the interpretation that the shifted eigenvalues in Table 4.3 are due to CM excitations.

Additionally, we may employ the virial theorem again to compute the lowest expected "physical" eigenvalue of Trel where the center of mass wavefunction must be in a 0S state. This only requires that $\frac{1}{2}(2n_{rel}+l_{rel}+\frac{3}{2})\hbar\Omega = \frac{1}{2}(0+2+\frac{3}{2})\hbar\Omega = 262.5$ MeV since $M_{tot} = M_{rel} = 2$. Hence our contention that the eigenvalue that remains unchanged after the application of Hcm belongs to a physical ground state with a 0S center of mass wavefunction and a relative wavefunction like $|\Psi_0\rangle = |0D, M=2\rangle_{rel} \otimes |0S, m=0\rangle_{cm}$ is supported.

Our next comparison case adds a linear confining interaction to the Hamiltonian. This can be seen in Table 4.4, and the positive shift in the eigenvalues is to be expected due to the type of interaction added. We should note that the color operator $-3/4\,\vec{\lambda}\bullet\vec{\lambda}$ multiplies all relative coordinate interaction terms in MFDq for these tests. For the $q\bar{q}$ system $\vec{\lambda}\bullet\vec{\lambda}$ yields a value of –4/3 in the color singlet channel which amounts to multiplying by a net factor of unity. This allows MFDq and MFDn to use the same values for the other Hamiltonian parameters. (This is in addition to adding $\kappa\vec{\lambda}\bullet\vec{\lambda}$ to the Hamiltonian in MFDq as stated in Table 4.3.)

Table 4.4: A systematic comparison of eigenvalues (in MeV) from MFDq and MFDn for case 4. Multiplicity is given in square brackets.

MFDn[a]	MFDq
1394.7 [3]	1394.7 [6]
2631.0 [4]	2631.0 [8]
3820.2 [3]	3820.2 [6]

[a] Here $H = Trel + \alpha H_{cm} + \sigma r$ in the case of MFDn and $\sigma = 500\,\text{MeV-fm}^{-1}$.

We now add a delta function interaction which acts only on states with S=1 and designate this test as "case 5" recorded in Table 4.5. This lifts some of the degeneracy we

have seen so far and allows a better understanding of the physical content of some of the states.

Table 4.5: A systematic comparison of eigenvalues (in MeV) from MFDq and MFDn for case 5. Multiplicity is given in square brackets.

MFDn [a]	MFDq
1394.8 [3]	1394.7 [6]
2631.0 [4]	2631.0 [8]
3820.2 [1]	3820.2 [2]
3833.9 [2]	3833.9 [4]

[a] Here $H = T_{rel} + \alpha H_{cm} + \sigma r + \beta_1 \delta(\vec{r}_{12})$ in the case of MFDn, where $\beta_1 = 12$ MeV-fm^3.

In fact, since we know that the wave functions for a harmonic oscillator are proportional to r^l near the origin, the delta function will affect only states with $l = 0$. This tells us that the highest eigenvalue in Table 4.5 belongs to a state with zero relative orbital angular momentum. All other states must have $l \neq 0$ or have S=0 to remain unaffected. The relative multiplicity between MFDq and MFDn remains at 2 for all states, as expected.

Our next comparison test, "case 6", adds a delta function term which acts only on states with S=0. If we refer to Table 4.6 below, it is easy to see that the S=0 delta function shifts only one of the eigenvalues, which tells us that the state belonging to that eigenvalue is a state of zero relative orbital angular momentum and S=0. The fact that the two lowest sets of eigenvalues remain unaffected informs us again that those states must have some relative orbital angular momentum. Since a $q\bar{q}$ must have either S=1 or S=0, this demonstrates conclusively that the unaffected states have l=1 or 2, the only allowed values in our 2 $\hbar\Omega$ basis space. Since a 2 $\hbar\Omega$ basis space requires even orbital parity, we deduce that the states unaffected by the delta function interactions have $l = 2$. As noted above, these states have 0S harmonic oscillator CM motion.

The sequential analysis of the states so far suggests that a spin-orbit and/or a tensor interaction will affect the eigenvalues that have remained constant under the action of the delta functions.

Table 4.6: A systematic comparison of eigenvalues (in MeV) from MFDq and MFDn for case 6. Multiplicity is given in square brackets.

MFDn [a]	MFDq
1394.8 [3]	1394.7 [6]
2631.0 [4]	2631.0 [8]
3813.3 [1]	3813.3 [2]
3833.9 [2]	3833.9 [4]

[a] Here $H = T_{rel} + \alpha H_{cm} + \sigma r + \beta_1 \delta(\vec{r}_{12}) + \beta_0 \delta(\vec{r}_{12})$ in MFDn, where $\beta_0 = -6.0\ \text{MeV-fm}^3$.

For illustrative purposes, we will add each in turn. For "case 7" we add a spin-orbit interaction adapted from Bethe [2].

$$V_{so} = \frac{1}{r^3} \vec{l} \bullet \vec{S}$$

$\vec{S}$ is the spin angular momentum. The spin-orbit interaction is very effective in splitting many states that were previously degenerate.

Table 4.7: A systematic comparison of eigenvalues (in MeV) from MFDq and MFDn for case 7. Multiplicity is given in square brackets.

MFDn [a]	MFDq
1393.2 [1]	1393.2 [2]
1394.8 [1]	1394.8 [2]
1397.8 [1]	1397.8 [2]
2627.2 [1]	2627.1 [2]
2631.0 [1]	2631.0 [2]
2634.9 [2]	2634.9 [4]
3813.3 [1]	3813.3 [2]
3833.9 [2]	3833.9 [4]

[a] Here $H = T_{rel} + \alpha H_{cm} + \sigma r + \beta_1 \delta(\vec{r}_{12}) + \beta_0 \delta(\vec{r}_{12}) + \eta V_{so}$, where $\eta = 10\ \text{MeV-fm}^3$.

Table 4.8: A systematic comparison of eigenvalues (in MeV) from MFDq and MFDn for case 8. Multiplicity is given in square brackets.

MFDn[a]	MFDq
1393.2 [1]	1393.2 [2]
1394.8 [1]	1394.8 [2]
1396.1 [1]	1396.1 [2]
2627.2 [1]	2627.2 [2]
2631.0 [1]	2631.0 [2]
2631.8 [2]	2631.8 [4]
3813.3 [1]	3813.3 [2]
3833.9 [2]	3833.9 [4]

[a] $H = T_{rel} + \alpha H_{cm} + \sigma r + \beta_1 \delta(\vec{r}_{12}) + \beta_0 \delta(\vec{r}_{12}) + \eta V_{so} + \omega V_{tens}$, where $\omega = 20$ MeV-fm^3.

We now add a tensor interaction for "case 8" modeled on its electromagnetic counterpart from Jackson [3].

$$V_{tens} = \frac{1}{r^3}\left[\vec{S}_1 \bullet \vec{S}_2 - 3(\vec{S}_1 \bullet \hat{r})(\vec{S}_2 \bullet \hat{r})\right]$$

The tensor term added to the Hamiltonian in Table 4.8 does not alter the degeneracy of the states involved. It should be pointed out that all eigenvalues that differed in Tables 4.5, 4.6, and 4.7 are now in agreement through 5 significant figures between MFDn and MFDq. This numerical imprecision at the .1 MeV level is unimportant in our physical applications. Essentially, these small differences in the fifth significant figure is probably due to some numerical imprecision introduced by rounding the sixth significant figure during computation. It is worth pointing out that this disagreement often disappears when interaction terms in the Hamiltonian are turned on. Hence this difference may be due to very slight differences in the numerical values of the matrix elements themselves, although this is unlikely.

The last interaction term to be introduced is the one gluon exchange interaction that is modeled by a Coulomb-like term, $V_{OGE} = -a/r$, and we designate this as "case 9". The effect of this attractive potential on the spectrum introduces additional shifts in the states.

Table 4.9: A systematic comparison of eigenvalues (in MeV) from MFDq and MFDn for case 9. Multiplicity is given in square brackets.

MFDn [a]	MFDq
1365.6 [1]	1365.6 [2]
1367.1 [1]	1367.2 [2]
1368.4 [1]	1368.5 [2]
2592.7 [1]	2592.6 [2]
2596.5 [1]	2596.5 [2]
2597.3 [2]	2597.3 [4]
3761.5 [1]	3761.5 [2]
3782.1 [2]	3782.1 [4]

[a] Here $H = T_{rel} + \alpha H_{cm} + \sigma r + \beta_1 \delta(\vec{r}_{12}) + \beta_0 \delta(\vec{r}_{12}) + \eta V_{so} + \omega V_{tens} - a/r$, with c= 40 MeV-fm. The value for "a" must be scaled by a factor of 1.439897, the electronic charge.

Our final test in this particular sequence of accuracy checks, "case 10", retains the Hamiltonian we have defined in Table 4.9 and simply changes the basis space to compute the spectrum for M=0. The number of available states is now increased since all J values are now allowed. The results are included below in Table 4.10. Note that the eigenvalues of the M=2 calculation are included as a subset of the M=0 eigenvalues and occupy the higher parts of the spectrum as expected of states with high J. Four states have appeared in the low-lying spectrum and the multiplicity of several high-lying states has either doubled or tripled compared to the M=2 results in Table 4.9. Note again that the double degeneracy between MFDn and MFDq still exists and, as before, can be attributed to an extra SU(2) flavor degeneracy in MFDq.

Table 4.10: A systematic comparison of eigenvalues (in MeV) from MFDq and MFDn for case 10. Multiplicity is given in square brackets.

MFDn [a]	MFDq
202.1 [1]	202.1 [2]
226.2 [1]	226.1 [2]
768.4 [1]	768.4 [2]
795.3 [1]	795.3 [2]
1357.1 [1]	1356.9 [2]
1365.6 [1]	1365.6 [2]
1367.1 [1]	1367.2 [2]
1368.4 [1]	1368.4 [2]
2558.4 [1]	2558.4 [2]
2592.7 [3]	2592.7 [6]
2596.5 [3]	2596.4 [6]
2597.3 [3]	2597.3 [6]
3761.5 [2]	3761.5 [4]
3782.1 [4]	3782.1 [8]

[a] Here we have the Hamiltonian as above in Table 4.9, but with M=0 instead of M=2 for the quark-antiquark basis states.

SHO Basis Space Properties for MFDn and MFDq

We complete this round of testing on the 2-body system by recording SHO basis state properties for MFDn and MFDq. These results do not depend on the particular Hamiltonian, but they serve as a useful comparison of performance between the two schemes for the 2-body problem. Table 4.11 presents data on the SHO basis space that is independent of the Hamiltonian and the number of particles in the many-body problem, and relies only on the set of quantum numbers employed by MFDn and MFDq. The labels NUMCLS and ndwd, defined below, are significantly larger for MFDq in large basis spaces. This becomes increasingly important since these parameters strongly affect the amount of storage space required for computation.

Table 4.12 shows performance data for MFDn and MFDq that compare the two schemes for a 2-body calculation similar to the ones performed during the earlier round of testing in Tables 4.1-10. The practical effects of including color and flavor degrees of freedom can be clearly seen, particularly in large basis spaces. The computational time required for MFDq grows far more rapidly than MFDn.

Table 4.11: SHO basis space properties for MFDn and MFDq through 10 major shells.

Common properties[a]				MFDn[b]		MFDq[b]	
SPS ID.	NSHEL	NSPS	MAXL	NUMCLS	ndwd	NUMCLS	ndwd
0s	1	1	0	2	1	12	1
0p	2	3	1	8	1	48	2
1s,0d	3	6	2	20	1	120	4
1p,0f	4	10	3	40	2	240	8
2s,1d,0g	5	15	4	70	3	420	14
2p,1f,0h	6	21	5	112	4	672	21
3s,2d,1g, 0i	7	28	6	168	6	1008	32
3p,2f,1h, 0j	8	36	7	240	8	1440	45
4S,3d,2g, 1i,0k	9	45	8	330	11	1980	62
4p,3f,2h, 1j,0l	10	55	9	440	14	2640	83

[a] SPS ID refers to which single particle oscillator states are allowed in the shell. NSHEL designates the number of oscillator shells allowed in the calculation. NSPS and MAXL are the number of single particle states and the maximum orbital angular momentum allowed, respectively.

[b] NUMCLS is the cumulative number of single particle states (including spin), and ndwd is the number of 32-bit words needed to encode a many-body state with one bit assigned to each single particle state.

Table 4.12: Dimensionality and run time performance for the even parity 2-body problem through 10 major shells.

Basis space	MFDn		MFDq	
N $\hbar\Omega$	Dimension of matrices	6 processor run time (seconds)	Dimension of matrices	6 processor run time (seconds)
0	2	20[a]	12	39
2	24	28	144	45
4	116	29	696	70
6	376	32	2256	173
8	966	53	5796	588
10	2128	96	12768	___[b]

[a] This run was performed on 1 processor. The number of processors must be less than the dimensionality of the matrices or the run will not execute.

[b] This run could not be completed due to a temporary limitation of disc space.

Limited 4-Body Tests of MFDq

Since there is no comparable treatment to MFDq for systems beyond the 2-body level at our disposal for comparison purposes, we must rely on tests where the results can be checked independently by some other means. These tests will verify that MFDq properly handles all possible matrix elements. In the 2-body cases just completed, we could only test that the quark-antiquark matrix elements were computed correctly. In the 4-body case under consideration quark-quark and antiquark-antiquark matrix elements are needed for a complete treatment of the problem. The three simple tests we will perform here seek to examine this issue.

Run 1 involves a direct consistency check of the spectrum of the pure color operator defined in equation 2.3 multiplied by a large positive constant, κ. Since the single particle Casimir operator yields an eigenvalue of –4/3, we add 2N/3 to all eigenvalues after the spectrum is computed (N is the number of particles.) This ensures that color singlets receive no overall shift in the spectrum and that all other color multiplets lie above the singlet states

Table 4.13: Summary of test case eigenvalues in the 4-body problem with MFDq. Eigenvalues are in MeV.

Run 1 $H=\kappa\vec{\lambda}^2/2$	Run 2 $H=\alpha(2N+L)\hbar\Omega$	Run 3 (**M**, 2N+L)[a]
0 (**1**)	0 (2N+L=0)	0 (**1**,0)
4500 (**8**)	2560 (2N+L=1)	2560 (**1**, 1)
9000 (**10** or **10***)	5120 (2N+L=2)	4500 (**8**, 0)
12000 (**27**)		5120 (**1**, 2)
		7060 (**8**, 1)
		9000 (**10** or **10***, 0)
		9620 (**8**, 2)
		11560 (**10** or **10***, 1)
		12000 (**27**, 0)
		14120 (**10** or **10***, 2)
		14560 (**27**, 1)
		17120 (**27**, 2)

[a] **Boldfaced numbers** refer to the color multiplet of the state. See text below.

by an amount $\frac{1}{2}\kappa\vec{\lambda}^2$. Hence, we expect to see zero eigenvalues for color singlets and discrete positive eigenvalues for non-singlets.

Run 2 involves only the use of the center of mass Hamiltonian previously defined. This will determine if the quark-quark and antiquark-antiquark matrix elements are being handled properly by a dynamical operator in our Hamiltonian.

Run 3 uses the pure color operator and center of mass interaction simultaneously. Since these two operators commute, we should see that the spectral results should just be linear combinations of the eigenvalues present in the separate spectra of the two previous tests. This places a strong limitation on the allowed eigenvalues of the third test. This approach has a further advantage since the spectrum of all these test cases can be predicted simply by resorting to the known spectrum of a center of mass SHO Hamiltonian and the color Casimir operator. For reference the color Casimir operator, $\vec{\lambda}^2$, yields an eigenvalue of 0, 3, 6, and 8 for the SU(3) color multiplets **1**, **8**, **10** or **10***, and **27**, respectively. These are the only color multiplets that possess states that satisfy the "total color charge rule" restrictions of equation 2.4. The results of these tests are recorded in Table 4.13. For these tests we have used $\kappa = 3000$ MeV, $\alpha = 2$ and $\hbar\Omega$ is 1280 MeV. The quark mass is 1490 MeV, but this is immaterial for these tests. One can readily see that the eigenvalues of Run 3 are simply sums of the eigenvalues from Run 1 and Run 2, completely in accordance with our expectations.

Summary and Conclusions

The development and testing of MFDq in Chapters 3 and 4 have laid the foundations for generating Hamiltonian spectra with an arbitrary number of quarks in basis spaces that are constrained only by computer storage limitations. We have seen that MFDn and MFDq agree on a large and important subset of problems that introduce a variety of interactions and basis spaces for the 2-body problem. A further series of self-consistency checks of MFDq in the 4-body problem has shown that MFDq, to all appearances, yields the proper spectrum. This series of tests on the 4-body problem is still underway and remains incomplete, but we

have sufficient confidence to present preliminary 4-body results from MFDq using a Hamiltonian with robust interactions in the next chapter.

References

[1] P. Navratil, J. P. Vary, and B. R. Barrett, Phys. Rev. C **62**,054311 (2000).

[2] H. A. Bethe and R. Jackiw, *Intermediate Quantum Mechanics*, (Addison-Wesley, Reading, 1997).

[3] J. D. Jackson, *Classical Electrodynamics*, (John Wiley & Sons, New York, 1975), 2nd ed.

5 MANY-BODY RESULTS

Introduction

In this chapter the results of many-body calculations using the MFDq and MFDn frameworks are presented for $c\bar{c}$ mesons and the $2c2\bar{c}$ exotic spectrum. One of the primary motivations, mentioned in Chapter 1, is to predict novel many-charmonium quark states that may be observable at RHIC in the near future.

Although the results obtained from MFDn in the 4-body case are not fully realistic for such systems with color degrees of freedom, it is instructive to compare MFDn with the eventual full treatment afforded by MFDq. The effect of the extra quark degrees of freedom on the spectrum of physical states can then be recognized.

We shall begin this study by analyzing the convergence properties of the low-lying states of many-body spectra for MFDn. This will afford an opportunity to quantify the consequences of the Pauli principle by comparing the 2-body and 4-body results for the relative kinetic energy operator. More importantly this analysis will provide a criterion that can be used to judge if there is net binding in the 4-body system relative to the threshold for disassembly into two free mesons.

Limited spectral results from MFDq in the 4-body problem will be presented. We shall then conclude by comparing the result of the 2-body spectra found by MFDn to other models that are available in the literature.

Rates of Convergence in 2-Body Spectra

In Chapter 3 we outlined the methods used to compute the spectrum of a general 2-body Hamiltonian. With the Lanczos method MFD is able, using sufficient iterations for a given basis space, to give results that are numerically converged for a set of low-lying eigenstates. Due to the finite size of the basis space, however, the resulting spectrum is not

the actual spectrum of the full Hamiltonian but approaches it from above as the basis space is enlarged. The goal of this section is to investigate how the spectrum converges to the actual spectrum of the Hamiltonian for low-lying states. This is accomplished by computing the Hamiltonian spectrum in basis spaces of increasing size and observing that the low-lying states become stable against inclusion of higher oscillator shells. We must be aware, however that the smallest basis space in which the low-lying states become stable may change with the Hamiltonian and the basis space scale $\hbar\Omega$. Thus, we will present two cases with slightly different Hamiltonian parameters and $\hbar\Omega$ to illustrate this feature. These Hamiltonians are realistic in the sense that the parameters are chosen to fit the low-lying $c\bar{c}$ spectrum. We shall also present a third Hamiltonian that incorporates a relative oscillator interaction that the other Hamiltonians do not have in order to further compare convergence properties with respect to the size of the basis space. With the exception of multiplicity, MFDn and MFDq give the same spectral fits in this 2-body case, and therefore the spectra presented in Tables 5.1-6 are produced by MFDn.

We note that here and throughout the thesis, results unless otherwise noted are presented as a sum of the binding energy calculated with the Hamiltonian and the rest masses of the constituent quarks. In this way, our results may be compared directly with the experimentally measured masses when they are available.

We also remind the reader of the nomenclature for the designation of the basis space. The designation "N $\hbar\Omega$" represents the largest excitation allowed in the basis space when we sum over the oscillator quanta (2n+l) of all the constituents. All basis states at or below this excitation, for a given total parity, are included in a result obtained in the "N $\hbar\Omega$" model space.

The Hamiltonian parameters were tuned to obtain the best fit for the combined set of results from the 10 $\hbar\Omega$ basis space in the even orbital parity spectrum and the 9 $\hbar\Omega$ basis space in the odd orbital parity spectrum. Each table shows that the two lowest states in the even orbital parity spectrum are nearing stability with respect to the size of the basis space. This indicates that the Hamiltonian parameters will require further adjustment as the basis space includes more SHO shells.

Table 5.1: Even orbital parity spectrum for $c\bar{c}$ with masses in MeV versus basis space for H_1 [a] with $\hbar\Omega = 1280$ MeV and $m_q = 1490$ MeV.

ID	J	T	M_{exp} [b]	$0\hbar\Omega$	$2\hbar\Omega$	$4\hbar\Omega$	$6\hbar\Omega$	$8\hbar\Omega$	$10\hbar\Omega$
$\eta_c(1S)$	0	1	2980	3537	3369	3203	3151	3092	3069
J/ψ	1	0	3097	4302	3466	3343	3198	3155	3097
$\eta_c(2S)$	0	1	3594	____	4854	4417	3995	3855	3676
$\psi(2S)$	1	0	3686	____	5164	4609	4327	4005	3878

[a] $H_1 = T_{rel} + \sigma r + \alpha H_{cm} + \beta_1\delta(\vec{r}_{ij}) + \beta_0\delta(\vec{r}_{ij}) + \eta V_{so} + \omega V_{tens} + a/r$. Parameter units are the same as in Chapter 4. $\sigma = 650, \alpha = 10, \beta_0 = 2.4, \beta_1 = -0.4, a = -55, \omega = \eta = 0.32$.

[b] All masses are taken from the Particle Data Book [1].

Table 5.2: Odd orbital parity spectrum for $c\bar{c}$ with masses in MeV versus basis space for H_1 [a] with $\hbar\Omega$=1280 MeV and m_q=1490 MeV.

ID	J	T	M_{exp} [b]	$1\hbar\Omega$	$3\hbar\Omega$	$5\hbar\Omega$	$7\hbar\Omega$	$9\hbar\Omega$
$\chi_{c0}(1P)$	0	1	3415	4311	4014	3719	3542	3423
$\chi_{c1}(1P)$	1	1	3511	4455	4062	3808	3638	3511
$h_c(1P)$	1	0	3526	4483	4071	3825	3656	3528
$\chi_{c2}(1P)$	2	1	3556	4498	4076	3834	3666	3537

[a] $H_1 = T_{rel} + \sigma r + \alpha H_{cm} + \beta_1\delta(\vec{r}_{ij}) + \beta_0\delta(\vec{r}_{ij}) + \eta V_{so} + \omega V_{tens} + a/r$ and the parameters are defined in Table 5.1.

[b] All masses are taken from the Particle Data Book [1].

Tables 5.3 and 5.4 show the results for a slightly different choice of Hamiltonian and basis space parameter, $\hbar\Omega$. It is apparent that, as with the previous Hamiltonian results in Tables 5.1 and 5.2, only the lowest two states in the even orbital parity spectrum are nearing stability with respect to increasing basis space size. The results for the $c\bar{c}$ spectrum in the 10 $\hbar\Omega$ basis space compare well in both cases to the experimentally determined spectrum

Table 5.3: Even orbital parity spectrum for $c\bar{c}$ with masses in MeV versus basis space for H_2 [a] with $\hbar\Omega$=1200 MeV and m_q=1500 MeV.

ID	J	T	M_{exp}	$0\hbar\Omega$	$2\hbar\Omega$	$4\hbar\Omega$	$6\hbar\Omega$	$8\hbar\Omega$	$10\hbar\Omega$
$\eta_c(1S)$	0	1	2980	4024	3352	3187	3152	3089	3074
J/ψ	1	0	3097	4024	3442	3320	3198	3155	3105
$\eta_c(2S)$	0	1	3594	____	4637	4301	3884	3783	3602
$\psi(2S)$	1	0	3686	____	5053	4545	4268	3943	3822

[a] $H_1 = T_{rel} + \sigma r + \alpha H_{cm} + \beta_1 \delta(\vec{r}_{ij}) + \beta_0 \delta(\vec{r}_{ij}) + \eta V_{so} + \omega V_{tens} + a/r$. Parameter units are as in Chapter 4. $\sigma = 650, \alpha = 10, \beta_0 = 1.6, \beta_1 = -0.6, a = -55, \omega = 0.32, \eta = 0.32$.

Table 5.4: Odd orbital parity spectrum for $c\bar{c}$ with masses in MeV versus basis space for H_2 [a] with $\hbar\Omega$=1200 MeV and m_q=1500 MeV.

ID	J	T	M_{exp}	$1\hbar\Omega$	$3\hbar\Omega$	$5\hbar\Omega$	$7\hbar\Omega$	$9\hbar\Omega$
$\chi_{c0}(1P)$	0	1	3415	4250	3982	3704	3536	3422
$\chi_{c1}(1P)$	1	1	3511	4384	4028	3788	3625	3503
$h_c(1P)$	1	0	3526	4417	4039	3808	3647	3523
$\psi(2S)$	2	1	3556	4440	4046	3822	3662	3537

[a] $H_1 = T_{rel} + \sigma r + \alpha H_{cm} + \beta_1 \delta(\vec{r}_{ij}) + \beta_0 \delta(\vec{r}_{ij}) + \eta V_{so} + \omega V_{tens} + a/r$. Parameters are defined in Table 5.3.

with the exception of the highest state in the even orbital parity spectrum in Tables 5.1 and 5.3. This is not a cause for concern since the rate of convergence for that state suggests that it will drop substantially as more oscillator shells are included in the calculation. The rates of convergence for the remaining states indicate that the Hamiltonian parameters may require adjustment to maintain an overall good fit to the $c\bar{c}$ spectrum when calculations are carried out in these larger basis spaces.

The two Hamiltonians we have employed so far are similar since they both share the same interactions, and they differ only in a choice of the strength parameters of those interactions. It is instructive to introduce a Hamiltonian which employs a different interaction entirely and forces the strength parameters of the Hamiltonian interactions to depend on only 4 independent parameters: The quark mass, the strong coupling constant, the linear confinement coupling and β, an adjustable delta function coupling defined in equation 5.1. The oscillator spacing, $\hbar\Omega$, is also a variable, but it is not treated as an adjustable parameter of the Hamiltonian. The form of the one gluon exchange (OGE) interaction Hamiltonian was taken from [2] with β=1. (We have inserted β for use as a free parameter to set the splitting between the 1S states.) Natural units with $\hbar$=c=1 are used in this expression.

$$
\begin{aligned}
H &= T_{rel} + U_{rel} + V_{OGE} - \vec{\lambda}_i \bullet \vec{\lambda}_j \left(\sigma r + \frac{3}{4} V_{so} \right) + \alpha H_{cm} \\
V_{OGE} &= \vec{\lambda}_i \bullet \vec{\lambda}_j \alpha_s \left[\frac{1}{r} - \beta \frac{\pi}{m^2} \left(1 + \frac{2}{3} \vec{\sigma}_i \bullet \vec{\sigma}_j \right) \delta(\vec{r}_{ij}) - \frac{3}{4} V_{tens} \right]
\end{aligned}
\tag{5.1}
$$

The expression in equation 5.1 is correct for our definition of the generators. All interaction terms not defined above are as in Chapter 4. The results for this Hamiltonian are recorded below in Tables 5.5 and 5.6 where we present results only in the largest model spaces since they are sufficient for our purposes. We may note that almost all states are essentially stable with respect to the basis space size. This is due to the fact that a relative harmonic oscillator interaction was included in the Hamiltonian. All other interaction terms, including the linear

confinement, are small enough relative to the quadratic oscillator interaction to be perturbative. Therefore, the eigenstates will have greater overlap with the low-lying oscillator shells than the eigenstates of the first two Hamiltonians in which the linear confinement interaction was the dominant long range potential. This realization explains the significantly different rates of convergence in Tables 5.5-6 compared to the earlier results in Tables 5.1-4.

Table 5.5: Even orbital parity spectrum for $c\bar{c}$ with masses in MeV versus basis space for H_3 [a] with $\hbar\Omega$=335 MeV and m_q=1330 MeV.

ID	J	T	M_{exp}	$0\hbar\Omega$	$2\hbar\Omega$	$4\hbar\Omega$	$6\hbar\Omega$	$8\hbar\Omega$	$10\hbar\Omega$
$\eta_c(1S)$	0	1	2980	____	____	____	3002	2993	2986
J/ψ	1	0	3097	____	____	____	3125	3125	3125
$\eta_c(2S)$	0	1	3594	____	____	____	3564	3557	3553
$\psi(2S)$	1	0	3686	____	____	____	3654	3654	3654

[a] H_3 is defined in equation 5.1 with $\sigma = 490, \alpha = 10, \beta = 1/9, \alpha_s = -75\text{MeV - fm}$. α_s is scaled by a factor of 1/1.439897.

Table 5.6: Odd orbital parity spectrum for $c\bar{c}$ with masses in MeV versus basis space for H_3 [a] with $\hbar\Omega$=335 MeV and m_q=1330 MeV.

ID	J	T	M_{exp}	$1\hbar\Omega$	$3\hbar\Omega$	$5\hbar\Omega$	$7\hbar\Omega$	$9\hbar\Omega$
$\chi_{c0}(1P)$	0	1	3415	____	____	____	3382	3382
$\chi_{c1}(1P)$	1	1	3511	____	____	____	3549	3548
$h_c(1P)$	1	0	3526	____	____	____	3584	3584
$\chi_{c2}(1P)$	2	1	3556	____	____	____	3599	3598

[a] H_3 is defined in equation 5.1 with $\sigma = 490, \alpha = 10, \beta = 1/9, \alpha_s = -75\text{MeV - fm}$.

A Net Binding Analysis in the 4-Body Problem

At this juncture in our analysis we need to choose some reasonable criteria to decide if the 4-body spectrum yields any bound states with respect to breakup into two separate $c\bar{c}$ mesons. The fact that our basis space is built out of harmonic oscillator states implies that all states will exhibit an appearance of being bound, but this is not sufficient to conclude that a solution actually corresponds to a physically bound state. To assess this complicated feature of our analysis, we compare the 2-body spectra of the relative kinetic energy operator to the 4-body spectrum of the full Hamiltonian in the following way.

$$\Delta M_{c\bar{c}c\bar{c}}^{free,N,\hbar\Omega} = M_{c\bar{c}c\bar{c}}^{free,N,\hbar\Omega} - \underset{n}{Min}[M_{c\bar{c}}^{free,n,\hbar\Omega} + M_{c\bar{c}}^{free,N-n,\hbar\Omega}] \tag{5.1}$$

M, regardless of subscripts or superscripts, denotes the mass of the indicated free particle system. This equation quantifies the kinetic energy penalty exacted by placing free particles in a finite basis. When we compute the spectra of the full Hamiltonian in the 4-body system, we will need to subtract the penalty in equation 5.1 from the results as follows.

$$M_{c\bar{c}c\bar{c}}^{corrected,N,\hbar\Omega} = M_{c\bar{c}c\bar{c}}^{H_{full},N,\hbar\Omega} - \Delta M_{c\bar{c}c\bar{c}}^{free,N,\hbar\Omega} \tag{5.2}$$

The 4-body spectra as corrected via equation 5.2 will then be compared to charmonium pairs from the 2-body bound state spectra in Tables 5.1-4, as appropriate, to decide if the 4-body state is physically bound by the full Hamiltonian. This determination relies mainly on mass considerations. In other words, to qualify as a bound exotic, the mass of the 4-body system must be less than the masses of any two-charmonium mesons to which it is allowed to decay. If this condition is satisfied, then the 4-body state will not decay via strong interactions to a final state of two charmed mesons. Decays involving electromagnetic or electroweak interactions are not considered since the lifetimes associated with those decays should be much longer than any decay mediated by the strong force. Thus such exotic 4-

body states become predictions for states with narrow decay widths to be seen in experiments such as the PHENIX detector experiments at RHIC.

The results for this analysis are tabulated below in Tables 5.7-14. The constituent quark masses are not included in the values reported in these tables as they cancel out in the analysis of $\Delta M_{cc\bar{c}\bar{c}}^{free,N,\hbar\Omega}$. That is, our Hamiltonians compute the excitation energy, and therefore the mass of the N-body state is just the sum of the excitation energy and N times the constituent quark mass. However, the constituent quark mass cancels in equations 5.1-2, leaving only the difference in excitation energy. For reference in Tables 5.1-6, the excitation energy can be obtained by subtracting twice the constituent quark mass from the values recorded in those tables.

Net binding analysis for case 1 with MFDn

Case 1 refers to the choice of quark mass, oscillator constant and Hamiltonian parameters made in Tables 5.1-2. Hence these free particle results below will be used to compute the kinetic energy penalty via equation 5.1. This penalty will then be used to correct the spectra computed by the Hamiltonian H_1 via equation 5.2. The final result for an N $\hbar\Omega$ 4-body state will then be compared to two 2-body states of (N-n) $\hbar\Omega$ and n $\hbar\Omega$ in Tables 5.1-2 to determine if there is any net binding in the 4-body system. The data for this is recorded in Tables 5.7-8.

We notice immediately all states in the 4-body spectrum gives indication of being bound with the exception of the two highest states at N=1. For example we note that the excitation is only 116 MeV at N=8 in Table 5.8. If this 4-body state decayed into two mesons, its excitation would lie above twice the excitation of the lowest-lying pair of states in the 2-body spectrum. The smallest possible excitation is 446 MeV from two N=4 2-body states. Since this is greater than the 4-body excitation of 116 MeV at N=8, we can safely conclude that the lowest-lying state in the 4-body spectrum is bound at N=8 by 330 MeV. A similar analysis reveals that all states in Table 5.8 are bound except as already noted.

Table 5.7: Lowest free particle spectra for 2-body and 4-body systems in N $\hbar\Omega$ basis spaces ($\hbar\Omega$ =1280 MeV, m_q =1490 MeV).

N=0	N=1	N=2	N=3	N=4	N=5	N=6	N=7	N=8	N=9
Lowest 2-body free particle spectra (MeV)									
960	1600	588	1043	426	781	335	626	276	523
Lowest 4-body free particle spectra (MeV) [a]									
2880	3520	2019	2528	1578	2006	1301	1672	1110	1437
NA	NA	4160	4780	3047	3574	2447	2901	2058	2548
$\Delta M_{cc\bar{c}\bar{c}}^{free,N,\hbar\Omega}$ as per equation 5.1 [b]									
960	960	471	525	402	375	287	303	187	230

[a] The next highest free particle 4-body state is recorded for reference purposes only.

[b] Values are computed only for the lowest 4-body free particle state.

Table 5.8: Raw and corrected 4-body spectrum systems for H_1 in N $\hbar\Omega$ basis spaces ($\hbar\Omega$ =1280 MeV, m_q =1490 MeV).

N=0	N=1	N=2	N=3	N=4	N=5	N=6	N=7	N=8	N=9
$M_{cc\bar{c}\bar{c}}^{H_{full},N,\hbar\Omega}$ [a]									
2757	2820	1311	1797	780	1411	500	1112	303	874
NA	3039	2485	1937	2097	1456	1722	1116	1464	890
NA	3167	2780	1981	2256	1525	1775	1158	1558	1010
$\Delta M_{cc\bar{c}\bar{c}}^{corrected,N,\hbar\Omega}$ as per equation 5.2 [b]									
1797	1860	840	1272	378	1036	213	809	116	671
	2079		1412		1081		813		687
	2207		1456		1150		855		707

[a] These are only the lowest three states for each N. The second state for N=9 is doubly degenerate.

[b] Values for the higher-lying states in the even parity spectrum were not computed since they are approximately 1 GeV above the lowest state and are therefore ignored. Only the the states of 2207 and 2079 MeV excitation at N=1 are unbound. Binding increases with increasing N for all states.

Net binding analysis for case 2 with MFDn

Case 2 refers to the choice of oscillator constant, quark mass and Hamiltonian parameters in Tables 5.3-4. The tables containing the necessary data are Tables 5.9-10.

Table 5.9: Lowest free particle spectra for 2-body and 4-body systems in N $\hbar\Omega$ basis space ($\hbar\Omega$=1200 MeV, m_q=1500 MeV).

N=0	N=1	N=2	N=3	N=4	N=5	N=6	N=7	N=8	N=9
Lowest 2-body free particle spectra (MeV)									
900	1500	551	977	400	732	314	587	259	491
Lowest 4-body free particle spectra (MeV) [a]									
2700	3300	1893	2370	1479	1880	1220	1567	1041	1347
NA	NA	3890	4500	2856	3351	2294	2720	1929	2304
$\Delta M_{cc\bar{c}\bar{c}}^{free,N,\hbar\Omega}$ as per equation 5.1 [b]									
900	900	442	493	377	352	269	284	241	215

[a] The next highest free particle 4-body state is recorded for reference purposes only.
[b] Values are computed only for the lowest 4-body free particle state.

The excitation for the 2-body states can be computed by subtracting 2*1500 MeV=3000 MeV from all values recorded in Tables 5.3-4. If we compare the corrected excitation in Table 5.10, we find that all 4-body state lies below any allowable pair of 2-body excitations derived from Tables 5.3-4. We see, for example, at N=8 that the 4-body state lies 51 MeV below the threshold of 4 constituent quark masses and is therefore a more deeply bound state than the corresponding Case 1 state for N=8. The negative parity states exhibit binding at N=1, and remain so for all N computed here. This indicates that the 4-quark charmonium system is more densely populated than previously realized. Since this conclusion is based on a color-blind treatment, however, we should not hasten to any conclusions and instead await more conclusive results from MFDq.

Table 5.10: Raw and corrected 4-body spectrum systems for H_2 in N$\hbar\Omega$ basis spaces ($\hbar\Omega$=1200 MeV, m_q=1500 MeV).

N=0	N=1	N=2	N=3	N=4	N=5	N=6	N=7	N=8	N=9
$M_{cc\bar{c}\bar{c}}^{H_{full},N,\hbar\Omega}$ [a]									
1790	2208	956	1568	570	1234	350	981	190	769
NA	2326	2191	1660	1904	1265	1557	985	1244	786
NA	2458	2518	1713	1975	1325	1566	1018	1306	871
$\Delta M_{cc\bar{c}\bar{c}}^{corrected,N,\hbar\Omega}$ as per equation 5.2 [b]									
890	960	514	1075	193	882	81	697	-51	554
	1426		1167		913		701		561
	1558		1220		973		734		656

[a] These are only the lowest three states for each N.

[b] Values for the higher-lying states in the even parity spectrum were not computed since they are approximately 1 GeV above the lowest state and are therefore ignored. All states recorded here are bound and increasingly so with increasing N.

Net binding analysis for Case 1 with MFDq

We present here some very preliminary results with MFDq in the 4-body problem for the Case 1 Hamiltonian. Due to temporary limitations in computer storage space, only results up to N=4 could be computed. We should note that the 4-body free particle spectrum is the same in MFDq as it is for MFDn. The spectra of the full Hamiltonian, however, differs significantly from MFDn and shows qualitative and quantitative differences with the spectral results of MFDn. For example, the low-lying positive parity 4-body spectrum for MFDq is heavily populated whereas in MFDn only one state was low in the spectrum, the first excited state being about 1 GeV higher. It is also apparent from comparison of Tables 5.7-10 with 5.11-14 that the lowest 4-body states of the full Case 1 Hamiltonian in MFDq lie above those of MFDn. This leads to the qualitative result that, at the present level of comparison, net binding is less in MFDq with a full treatment of color than in MFDn with a color-blind approach.

We can see that there is some net binding indicated for Case 1. In Table 5.12, the two lowest states are bound at N=0 and N=2, and all three lowest states are bound at N=4. The binding is shallower than MFDn predicts but it still exists.

Table 5.11: Lowest free particle spectra for 2-body and 4-body systems in N$\hbar\Omega$ basis space ($\hbar\Omega$=1280 MeV, m_q=1490 MeV).

N=0	N=1	N=2	N=3	N=4	N=5	N=6	N=7	N=8	N=9
Lowest 2-body free particle spectra (MeV)									
960	1600	588	1043	426	781	335	626	276	523
Lowest 4-body free particle spectra (MeV)[a]									
2880		2019		1578					
7380		4160		3047					
$\Delta M_{cc\overline{cc}}^{free,N,\hbar\Omega}$ as per equation 5.1[b]									
960		471		402					

[a] The next highest free particle 4-body state is recorded for reference purposes only.
[b] Values are computed only for the lowest 4-body free particle state.

Table 5.12: Raw and corrected 4-body spectrum systems for H_1 in N$\hbar\Omega$ basis spaces ($\hbar\Omega$=1280 MeV, m_q=1490 MeV).

N=0	N=1	N=2	N=3	N=4	N=5	N=6	N=7	N=8	N=9
$M_{cc\overline{cc}}^{H_{full},N,\hbar\Omega}$ [a]									
1462		1179		801					
1909		1306		927					
2292		1490		1035					
$\Delta M_{cc\overline{cc}}^{corrected,N,\hbar\Omega}$ as per equation 5.2									
502		708		399					
949		835		525					
1332		1019		633					

[a] These are only the lowest three states for each N.

Net binding analysis for Case 2 with MFDq

Table 5.13: Lowest free particle spectra for 2-body and 4-body systems in N$\hbar\Omega$ basis space ($\hbar\Omega$=1200 MeV, m_q=1500 MeV).

N=0	N=1	N=2	N=3	N=4	N=5	N=6	N=7	N=8	N=9
Lowest 2-body free particle spectra (MeV)									
900		551		400					
Lowest 4-body free particle spectra (MeV) [a]									
2700		1893		1479					
7193		3900		2856					
$\Delta M_{cc\bar{c}\bar{c}}^{free,N,\hbar\Omega}$ as per equation 5.1 [b]									
900		442		377					

[a] The next highest free particle 4-body state is recorded for reference purposes only.
[b] Values are computed only for the lowest 4-body free particle state.

Table 5.14: Raw and corrected 4-body spectrum systems for H_2 in N$\hbar\Omega$ basis spaces ($\hbar\Omega$=1200 MeV, m_q=1500 MeV).

N=0	N=1	N=2	N=3	N=4	N=5	N=6	N=7	N=8	N=9
$M_{cc\bar{c}\bar{c}}^{H_{full},N,\hbar\Omega}$ [a]									
1519		1196		854					
1870		1320		974					
2146		1458		1068					
$\Delta M_{cc\bar{c}\bar{c}}^{corrected,N,\hbar\Omega}$ as per equation 5.2									
619		754		477					
970		878		597					
1246		1016		691					

[a] These are only the lowest three states for each N.

One might recall that Case 2 exhibited binding for all N with MFDn. This is also true with MFDq. However the trend line in MFDq indicates the binding becomes shallower with

increasing N. For example at N=0 the highest state in Table 5.14 is bound by 1002 MeV, but by N=4 it is bound by 13 MeV. It is too early to say what the final net binding, if any, will be since our calculations in small N are insufficient to establish a more general trend with increasing N. This contrasts with the MFDq treatment of Case 1, which may be due to some sensitivity to the delta function or spin-orbit and tensor interaction parameters.

Other Capabilities of MFD

The graph below, produced by MFDn with the Case 3 Hamiltonian, shows the spin-averaged (uncorrelated) 2-body density for a quark-quark pair in an excited state of a 4-body system with the different curves showing the results for basis spaces of increasing size in the odd parity spectrum. We also show a similar graph for quark-antiquark pairs in the same excited state.

The spin-correlated graphs are not shown since this capability is still under development [8]. The graph of the quark-quark density shows a "shoulder" in the 2-body distribution starting at around 0.6 fm. In the quark-antiquark graph at this same separation, the 9 $\hbar\Omega$ curve shows a positive curvature where the smaller basis spaces indicate a negative curvature. In an extreme case of quark-antiquark pairing into two nearly free mesons, one would expect an enhancement in the quark-antiquark graph near zero relative separation and also at some larger separation coupled with a significant presence of quark-quark pairing at some distance beyond zero relative separation. This is not exactly what we see because the quark-quark pairing remains large near zero relative separation. However the quark-quark pairing between 0.5 fm and 1 fm is not insignificant and suggests that some degree of clustering has occurred.

MFD has the ability to produce 1-body densities as a function of distance from the center of mass, and 2-body densities as a function of relative separation for both spin-correlated and spin-averaged cases. When combined with the information gained from spin-correlations, a clear picture of the spatial configuration and spin composition of these clusters may emerge.

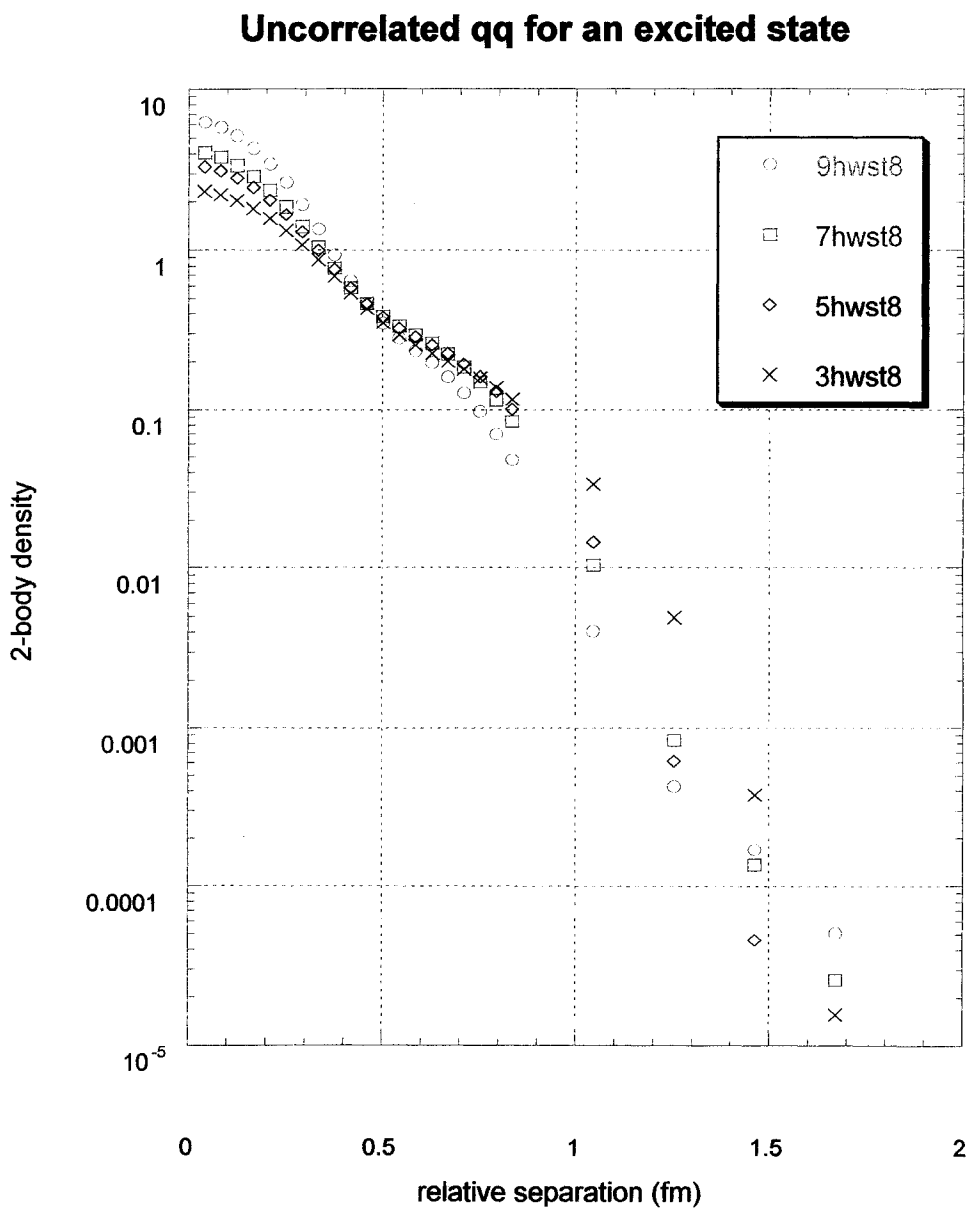
Uncorrelated qq for an excited state
10
1
0.1
0.01
0.001
0.0001
10^{-5}
2-body density
0
0.5
1
1.5
2
relative separation (fm)
9hwst8
7hwst8
5hwst8
3hwst8

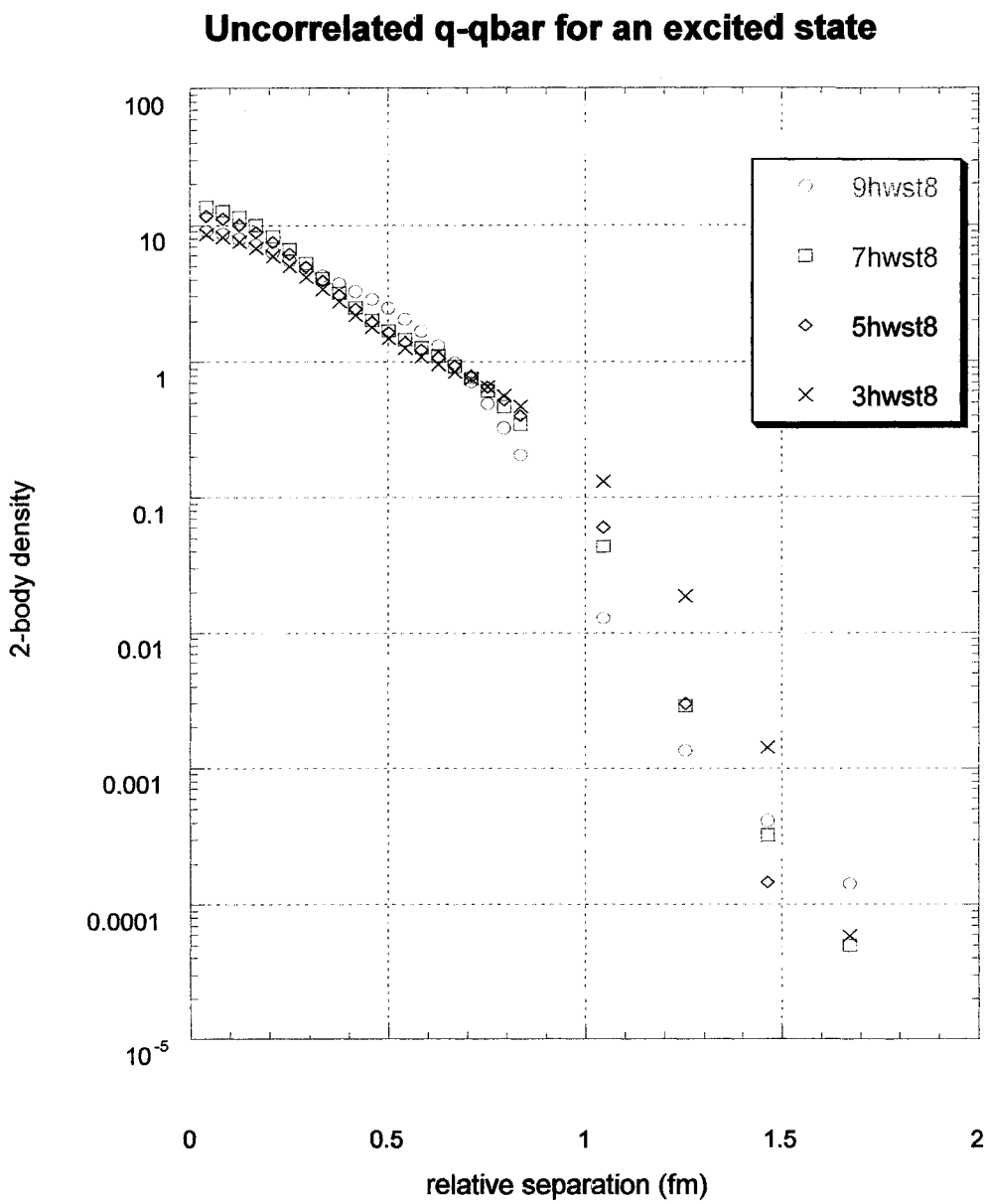
Uncorrelated q-qbar for an excited state
100
10
1
0.1
0.01
0.001
0.0001
10^{-5}
2-body density
0
0.5
1
1.5
2
relative separation (fm)
9hwst8
7hwst8
5hwst8
3hwst8

Comparison of Case 2 Hamiltonian Spectra to Other Models

We conclude this chapter with a brief comparison of various models that predict the charmonium spectrum. To be fair, all of these models have been applied to meson systems beyond charmonium, typically with fair to very good success. It is not our intention to claim that our Hamiltonian of Case 2 has validity beyond charmonium. Rather we make this comparison to prove a less sweeping point, that since our Case 2 Hamiltonian compares well with the various models in the charmonium system, we have some confidence that the 4-body results are not completely unrealistic. It should be mentioned that there are no 4-body many-charm results in the literature with which we can compare.

As can easily be seen from Table 5.11, with the exception of $\eta_c(2S)$, our Case 2 Hamiltonian compares well to the results of these other popular models.

Table 5.11: Comparison of various models of the charmonium 2-body system.

ID	Exp.	CCD[a]	BS[b]	GI[c]	WISC[d]	Case 2
$\eta_c(1S)$	2980	2978	3011	2970	2967	3074
J/ψ	3097	3129	3129	3100	3167	3105
$\eta_c(2S)$	3594	3610	3580	3620	3621	3602
$\psi(2S)$	3686	3688	3680	3680	3668	3822
$\chi_{c0}(1P)$	3415	3407	3410	3440	3402	3422
$\chi_{c1}(1P)$	3511	3507	3498	3510	3493	3503
$h_c(1P)$	3526	3520	3514	3520	____	3523
$\chi_{c2}(1P)$	3556	3549	3540	3550	3548	3537

[a] Covariant constraint dynamics by Alstine and Crater [3].
[b] Brayshaw [4].
[c] Godfrey and Isgur [5].
[d] Gara, Durand, and Durand [6].

Summary and Conclusions

We have seen that a satisfactory fit to the low-lying charmonium spectrum is given by several of our model Hamiltonians. The fits of charmonium provided by all of these Hamiltonians compare well to other, more widely applicable models available in the literature on this restricted subset of the meson spectra.

The two Hamiltonians we used to compute the 4-body spectra using MFDn both found, via the net binding analysis, the lowest bound state in the positive parity spectrum. Thus, we make an initial prediction of an exotic many-charm system. This result is encouraging but will not be definitive until these results are confirmed by further calculations using MFDq and other Hamiltonians such as that in Ref. [7].

With our present results, we can also take the average of the two cases for the lowest bound state to predict an average value of the theoretical mass of 6.033 GeV with a deviation of about .084 GeV from the mean. The total angular momentum of the state is J=0.

References

[1] Review of Particle Physics, D. E. Groom et al., The European Physical Journal **C15** (2000).

[2] B. Julia-Diaz, F. Fernandez, P. Gonzalez and A. Valcarce, Phys. Rev. C **63** (2001).

[3] H. Crater and P. Van Alstine, hep-ph/020816

[4] D. D. Brayshaw, Phys. Rev. D **36**, 1465 (1987).

[5] S. Godfrey and N. Isgur, Phys. Rev. D1 **32**, 189 (1985).

[6] A. Gara, B. Durand and L. Durand, Phys. Rev. D1 **42**, 1651 (1990).

[7] J. R. Spence and J. P. Vary, Phys. Rev. C, (submitted 2003).

[8] The algorithm and FORTRAN code implementation was kindly provided by O. Atramentov.

6 SUMMARY AND OUTLOOK

The spectroscopy of 4-quark systems has received little attention in theoretical circles in recent years. This has been generally due to expectations sharpened by experience with the light quark sector of hadron theory. Most theoretical predictions of 4-quark bound states have shown very little binding and are typically not stable against an immediate breakup into a pair of constituent mesons. Some of the viable 4-quark candidates mentioned in Chapter 1 seem to vindicate this view, especially the $f_0(980)$ and $a_0(980)$ that sit on the breakup threshold of two K mesons. One of the primary interests for future research is to investigate whether the expectation that 4-quark states are not stable against breakup into a pair of free mesons can be maintained in the heavy quark sector. The results of Chapter 5, although preliminary, suggest that there may indeed be quasi-stable heavy 4-quark states.

We intend to pursue the calculations of 4-quark states demonstrated in Chapter 5 until the spectroscopy becomes fully stable against increasing the size of the basis space. When completed we will be able to analyze the resulting states via the spin-correlated 2-body and 1-body density functions – initially within the color-blind approximation of MFDn. This enables a simple and practical determination of the physical sub-structure of the 4-body state. For example, if quark-antiquark clustering is observed in the 2-body correlations we will be able to investigate the spin composition of these meson-like sub-structures. In other words, we will be able to determine if the 4-quark state is dominated by a configuration resembling two J/ψ mesons bound together, for example. This will certainly be important for the experimental efforts when invariant mass distributions of the possible decay products are examined. However this analysis will not be definitive because our initial correlation functions are not yet able to specify the color quantum number content of these sub-structures. This is important because the color structure of any meson-like clustering will affect the decay modes of these 2- body sub-structures. It is conceivable that quark-antiquark substructures may be dominated by the color octet configuration, which

inhibits the normal decay channels that are the signature of the charmonium mesons. In this case, quark-antiquark annihilation processes to gluons would likely dominate the decay modes. This would lead to a naïve expectation that the 4-quark state decays would lead to final states of glueballs and/or hybrid states (bound states of gluons and quark-antiquark). Hence, we will then pursue the full implementation of correlation function evaluations within MFDq, treating the color degree of freedom more fully.

Future additional developments of MFDq will incorporate the use of a kinematically relativistic Hamiltonian so that we may extend our treatment to the light quark sector. Of course we are fully capable of addressing systems with arbitrary numbers of quarks and antiquarks including the pentaquark system. We can then undertake a systematic examination of many-quark spectroscopy in the light and heavy quark sectors that is limited only by practical computer storage and the restriction to no more than two flavors of quark that can be treated as having identical masses. This rules out for the present time using MFDq to compute a 3-quark state like uds, for example.

The immediate future will see an application of MFDq to the 4-quark charmonium system using a non-relativistic set of Hamiltonians outlined in Chapter 5. The results of these calculations will be used to make predictions of 4-quark bound states and provide a baseline comparison for the relativistic treatment. We hope that, if our results of a predicted quasi-bound state remain as suggestive as the preliminary calculations indicate, a renewed interest in many-quark bound states and their properties will lead to a deeper understanding of bound states in hadronic physics.

APPENDIX THE HAM SUBROUTINE OF MFD

This appendix seeks to document and to some extent explain the inner workings of the main subroutine of MFDq. Comments have been interspersed throughout to interpret and clarify the variables used and the logic employed. The computer code is usually single spaced to distinguish it from the other text that accompanies this appendix.

Function ham interfaces the shell-model code with effective quark-quark and quark-antiquark interactions. The integers II, JJ, KK, LL are unique binary sequence numbers for single particle fermion states. The Hamiltonian matrix elements <II JJ| H |KK LL> are computed and stored in this subroutine for all Hamiltonian operators. Variable "ham" is a Hamiltonian matrix element of an N-body state. Variables "hamcld", "hamcle", and "hamcli" are the color operators for the direct, exchange and identity operations, respectively. For example, T_{rel} is an operator multiplied by "hamcli", since T_{rel} is color-blind. The values below are initializations only and get reset as necessary throughout this subroutine.

For an off-diagonal matrix element of the Hamiltonian, the only difference between the two-body matrix element results returned by this subroutine and the full many-body matrix element is a phase factor computed by the calling program. The phase factor accounts for the anti-commutations necessary to position the two initial and final particles in the ordered list of fermions comprising the initial and final many-body states. In the case of a diagonal matrix element the phase factor is always +1 but there is a double sum over the two fermions created/annihilated in the initial and final state. For the case of a single particle scattered between the initial and final many-body state, there is a single sum over the non-scattered partner that runs through all the "spectator" fermions in the state. Here, the phase computation is straightforward and again simply reflects the rules of anticommutation relations.

```
c     function ham
ham = 0.0
```

```
hamcld = 0.0
hamcle = 0.0
hamcli = 0.0
hamcl = 0.0
haml = 0.0
```

ID array variable "5" (m2a, m2b, etc.) is the magnetic projection of the total angular momentum of a single particle state denoted by "ii", "jj", etc. The ID array stores the single particle identifiers defined in Chapter 3. The following conditions test that the magnetic projections of the total angular momentum and the isospin (itz2a, variable "7" for example) are the same for the final and initial states. The variables "lla", etc. are the orbital angular momenta of the single particle states as indicated by the ID array variable "2". The test on the "isgn(a)" variable (where "isgn(a)= $(-1)^a$) enforces parity conservation.

```
m2a  = ID(itrack(ii),icount(ii),5)
m2b  = ID(itrack(jj),icount(jj),5)
m2c  = ID(itrack(kk),icount(kk),5)
m2d  = ID(itrack(ll),icount(ll),5)
mmjj = m2a + m2b

if(mmjj.ne.(m2c+m2d))return
   itz2a = ID(itrack(ii),icount(ii),7)
   itz2b = ID(itrack(jj),icount(jj),7)
   itz2c = ID(itrack(kk),icount(kk),7)
   itz2d = ID(itrack(ll),icount(ll),7)
   mmtt = itz2a + itz2b
   if(mmtt.ne.(itz2c+itz2d))return
   lla  = ID(itrack(ii),icount(ii),2)
   llb  = ID(itrack(jj),icount(jj),2)
   llc  = ID(itrack(kk),icount(kk),2)
   lld  = ID(itrack(ll),icount(ll),2)

  if(isgn(lla+llb).ne.isgn(llc+lld))return
```

The step below converts II, JJ, KK, LL to sequence numbers understood by FNOSC, a subroutine of MFD that retrieves stored matrix elements in the harmonic oscillator basis in the coupled J and T scheme. For MFDq, these matrix elements have been previously computed according to the formulas given in Chapter XX of the thesis, with relative motion

integrals computed separately for each operator in the Hamiltonian. The matrix elements are in a direct product basis (no antisymmetrization) and are retrieved from stored arrays by the Subroutine FNOSC.

The following test checks for baryon number conservation since all Hamiltonian interactions conserve it. The symbol "ibary" denotes ID array variable "11", the baryon number for a 2-body state. This allows us to easily distinguish between quarks and antiquarks. Then we determine the phase (iphz) for a quark-quark or antiquark-antiquark versus a quark-antiquark color matrix element. See Chapter 2 for details.

```
      n(1) = ntrans(ii)
      n(2) = ntrans(jj)
      n(3) = ntrans(kk)
      n(4) = ntrans(ll)
     ibary = id(itrack(ii),icount(ii),11) + id(itrack(jj), icount(jj),11)
     if(ibary .ne. id(itrack(kk),icount(kk),11) +id(itrack(ll), icount(ll),11) )return
     iphz = -1
      if(ibary.ne.0) iphz = 1
```

The following sequence computes the pure color space matrix elements for quark-quark or antiquark-antiquark. The do loop checks that all the non-color quantum numbers (ID array variables 1-8) are the same before proceeding. The test following the do loop verifies that that the baryon numbers of the initial and final particles are the same. This checks to see if the direct matrix element contribution of the color operator may be non-zero.

```
      iidrct = 0
      do 4 i = 1,8
      if(id(itrack(ii),icount(ii),i).eq.id(itrack(kk),icount(kk),i)
     &  .and.
     &   id(itrack(jj),icount(jj),i).eq.id(itrack(ll),icount(ll),i))
     &  go to 4
        go to 5
4           continue
      if(id(itrack(ii),icount(ii),11).eq.id(itrack(kk),icount(kk),11)
     &  .and.
     &   id(itrack(jj),icount(jj),11).eq.id(itrack(ll),icount(ll),11))
     &  iidrct = 1
```

This step checks that the color quantum numbers Y and I^3 defined in Chapter 2 (ID array variables 9 and 10) of the final and initial particles are the same for the terms of the direct matrix element (cf. Chapter 2). Then the sign of the color operator matrix element, "ham", is set to the appropriate sign and the color identity operator, "hamcli", is set to 1 if the test is satisfied.

cjvv First term of direct color matrix element for either qq or q-qbar cases

```
 5          if(  id(itrack(ii),icount(ii),9)     .eq.
   &        id(itrack(kk),icount(kk),9) .and.
   &        id(itrack(ii),icount(ii),10)    .eq.
   &        id(itrack(kk),icount(kk),10).and.
   &        id(itrack(jj),icount(jj),9)     .eq.
   &        id(itrack(ll),icount(ll),9) .and.
   &        id(itrack(jj),icount(jj),10)    .eq.
   &        id(itrack(ll),icount(ll),10) ) then
     ham = -1. * iphz
     hamcli = 1.0
     endif
```

The condition "ibary=0" for a 2-body matrix element tells us we must compute the color matrix element for an antiquark-antiquark matrix element which must be handled separately from the case above. Of course only the direct term contributes in this case. The variable "hamcld" is the direct color matrix element and is scaled by a factor of 1/6 to conform to the definitions in Chapter 2. The variable "hamcl" is the color matrix element, which is set equal to "hamcld" for antiquark-antiquark.

```
     if(ibary.eq.0) go to 12
c    Check if there is a contribution from the second term
c    of the qq case to the direct color matrix element - evaluate it
       if(  id(itrack(ii),icount(ii),9)     .eq.
   &        id(itrack(ll),icount(ll),9)     .and.
   &        id(itrack(ii),icount(ii),10)    .eq.
   &        id(itrack(ll),icount(ll),10)    .and.
   &        id(itrack(jj),icount(jj),9)     .eq.
   &        id(itrack(kk),icount(kk),9)     .and.
   &        id(itrack(jj),icount(jj),10)    .eq.
   &        id(itrack(kk),icount(kk),10) ) ham = ham + 3.0

     go to 16
```

```
c    Arriving here means we check for contribution of second term
c    of the direct color matrix element for quark-antiquark case.

 12      continue

      if(  id(itrack(ii),icount(ii),9)     .eq.
     &       iphz*id(itrack(jj),icount(jj),9) .and.
     &       id(itrack(ii),icount(ii),10)    .eq.
     &       iphz*id(itrack(jj),icount(jj),10).and.
     &       id(itrack(kk),icount(kk),9)     .eq.
     &       iphz*id(itrack(ll),icount(ll),9) .and.
     &       id(itrack(kk),icount(kk),10)    .eq.
     &       iphz*id(itrack(ll),icount(ll),10) ) ham = ham - 3.0

 16      continue

c***  Finished evaluating the matrix element  of lambda dot lambda
c***  in the product space for the direct matrix element.

      hamcld = ham/6.0
       hamcl = hamcld
```

We now compute the exchange matrix element, and the procedure employed is generally the same as already presented. The only difference is that we must do this for identical exchanged particles. This is why we set kktem=kk, lltem=ll, and then switch the single particle identifiers. Everything else is a copy of the above procedure.

```
      ham = 0.0
c    determine phase for qq vs q-qbar matrix element
      iphz = -1
ctst        iphz=1
      if(ibary.ne.0) iphz = 1
      kktem = kk
      lltem = ll
      kk = ll
      ll = kktem

c***  Following for the pure color space matrix elements
      iiexch = 0
    do 400 i = 1,8
      if(id(itrack(ii),icount(ii),i).eq.id(itrack(kk),icount(kk),i)
     &  .and.
     &   id(itrack(jj),icount(jj),i).eq.id(itrack(ll),icount(ll),i))
```

```
   &  go to 400
      go to 450
 400     continue
      if(id(itrack(ii),icount(ii),11).eq.id(itrack(kk),icount(kk),11)
   &  .and.
   &   id(itrack(jj),icount(jj),11).eq.id(itrack(ll),icount(ll),11))
   &  iiexch = 1
 450       continue

    if(ibary.eq.0) go to 1650

c    Evaluate contribution for the exchange color matrix element

cjvv  test write
cjv      write(8,495)ii,jj,kk,ll
cjv 495     format(1x,'evaluating first term', 4i5)
cjvv

cjvv  Evaluate first term of exhange matrix element for either qq
cjvv  or qbar-qbar cases [Note that "kk" and "ll" have been interchanged
cjvv  above so statements appear in same form as direct mx el tests.
 500    hamclie = 0.0
       if(  id(itrack(ii),icount(ii),9)     .eq.
   &        id(itrack(kk),icount(kk),9) .and.
   &        id(itrack(ii),icount(ii),10)    .eq.
   &        id(itrack(kk),icount(kk),10).and.
   &        id(itrack(jj),icount(jj),9)     .eq.
   &        id(itrack(ll),icount(ll),9) .and.
   &        id(itrack(jj),icount(jj),10)    .eq.
   &        id(itrack(ll),icount(ll),10) ) then
       ham = -1. * iphz
       hamclie = 1.0
       endif

 600         continue

c    Check if there is a contribution from the second term
c    of the qq case to the exchange matrix element - evaluate it
       if(  id(itrack(ii),icount(ii),9)     .eq.
   &        id(itrack(ll),icount(ll),9)    .and.
   &        id(itrack(ii),icount(ii),10)   .eq.
   &        id(itrack(ll),icount(ll),10)   .and.
   &        id(itrack(jj),icount(jj),9)    .eq.
   &        id(itrack(kk),icount(kk),9)    .and.
   &        id(itrack(jj),icount(jj),10)   .eq.
```

```
     &        id(itrack(kk),icount(kk),10) ) ham = ham + 3.0

c       go to 1600
c    Arriving here means we check for contribution of second term
c    of the exchange matrix element for quark-antiquark case.
c 1200   continue
c       if(  id(itrack(ii),icount(ii),9)     .eq.
c    &        iphz*id(itrack(jj),icount(jj),9) .and.
c    &        id(itrack(ii),icount(ii),10)    .eq.
c    &        iphz*id(itrack(jj),icount(jj),10).and.
c    &        id(itrack(kk),icount(kk),9)     .eq.
c    &        iphz*id(itrack(ll),icount(ll),9) .and.
c    &        id(itrack(kk),icount(kk),10)    .eq.
c    &        iphz*id(itrack(ll),icount(ll),10) ) ham = ham - 3.0
c 1600   continue

 1650       kk = kktem
        ll = lltem
cjv   hamcle is the exchange matrix element of pure color operator
        hamcle = ham/6.0
        ham = 0.0
```

The step above is the end of the color matrix element evaluation for all cases: quark-quark, quark-antiquark, and antiquark-antiquark. Below, we take the Hamiltonian matrix elements in the coupled J,T basis and uncouple them to the m-scheme. The symbols "nna", "j2a", "it2a" (ID array variables 1, 4, and 6),etc. refer to the principal oscillator quantum number, the total angular momentum, and the total isospin for the single particle states, respectively. The symbols "wiga" and "wigb", etc. refer to the Wigner 3-j coefficients needed for this uncoupling transformation. Reference Chapter 3.

```
c    Retrieve the two-body matrix elements of the Hamiltonian in coupled form.
     call fnoscs
cjv  Special for the quark applications with files created storing the
cjv  "nucleon-like" quantum numbers, we need the following change
     jde = 1
     nna  = ID(itrack(ii),icount(ii),1)
     nnb  = ID(itrack(jj),icount(jj),1)

cjv  End of special change to accomodate quarks with these files.

if((nimj(1)+nimj(2)).eq.0)return
```

```
c     perform the uncoupling transformation

      j2a  = ID(itrack(ii),icount(ii),4)
      it2a = ID(itrack(ii),icount(ii),6)

      j2b  = ID(itrack(jj),icount(jj),4)
      it2b = ID(itrack(jj),icount(jj),6)
      nnc  = ID(itrack(kk),icount(kk),1)
      j2c  = ID(itrack(kk),icount(kk),4)
      it2c = ID(itrack(kk),icount(kk),6)
      nnd  = ID(itrack(ll),icount(ll),1)
      j2d  = ID(itrack(ll),icount(ll),4)
      it2d = ID(itrack(ll),icount(ll),6)

cjv   Compute the spectator oscillator quanta above minimum
      XNET = XNTOTO - FLOAT(2*nnc + llc + 2*nnd + lld)
      XNET = AMAX1(XNET,0.0)

      phsj = real(isgn((j2a-j2b+j2c-j2d)/2+80))
cjvv     compute the product of the quark charges
      q1q2 = float(itz2a)/2. + float(id(itrack(ii), icount(ii),11))/6.
      q1q2 = q1q2*(float(itz2b)/2.
     &       + float(id(itrack(jj), icount(jj),11))/6.)

cjvv    turn on "Coulomb" = one-gluon exch. for all isospin cases
cjvv    depending on value of str(3)

      indx = indx - 1

crl    Following phase is significant as it manages the possibility
crl    that the direct product matrix element is stored "flipped over"
crl    from the order requested here.
       iphsav = iphsb**((j2a+j2b)/2) * iphsk**((j2c+j2d)/2)

crl    Test for qbar-qbar of the same flavor:
       if(ibary.eq.-2.and.iabs(mmtt).eq.2)then
       if(nimj(2).eq.0)go to 320
       indx = indx + nimj(1)

       jval = j(2)-jde
       do 20 ij = 1,nimj(2)
         jval = jval + jde
         indx = indx + 1
         jjval = jval + jval
```

```
        if(IABS(mmjj).gt.jjval)go to 20

        wiga = wig3jr(j2a,j2b,jjval,m2a,m2b,-mmjj)
        wigb = wig3jr(j2c,j2d,jjval,m2c,m2d,-mmjj)

crl  str(3)  = strength of V_oge term
crl  str(5)  = strength of S=1 delta function
crl  str(12) = strength of S=0 delta function
crl  str(6)  = strength of V_coul
crl  xful( ) = Linear Confining + Spin-orbit + Tensor (see FNOSCS)
ham = ham + real((jjval+1)*iphsav)
   &        *wiga*wigb*(gfulnn(indx)*hamcli
   &        + str(3)*cful(indx)*hamcl
   &        - hamcl*
   &          (str(5)*rful(indx)+str(12)*rful2(indx))
   &        + str(6)*q1q2*cful(indx)*hamcli
   &        - hamcl*xful(indx)  )

 20    continue

      if(id(itrack(ii), icount(ii),11).ne.
   &     id(itrack(jj), icount(jj),11))go to 320

crl  Compute/add exchange term for identical particle case
crl  Antisymmetrization is the simple difference of a direct
crl  and an exchange matrix element.

    n(3) = ntrans(ll)
    n(4) = ntrans(kk)
    call fnoscs

    iphsav = iphsb**((j2a+j2b)/2) * iphsk**((j2c+j2d)/2)

    indx = indx - 1

      if(nimj(2).eq.0)go to 320
      indx = indx + nimj(1)

      jval = j(2)-jde
      do 70 ij = 1,nimj(2)
        jval = jval + jde
        indx = indx + 1
        jjval = jval + jval
        if(IABS(mmjj).gt.jjval)go to 70
```

```
        wiga = wig3jr(j2a,j2b,jjval,m2a,m2b,-mmjj)
        wigb = wig3jr(j2d,j2c,jjval,m2d,m2c,-mmjj)

crl  str(3)  = strength of V_oge term
crl  str(5)  = strength of S=1 delta function
crl  str(12) = strength of S=0 delta function
crl  str(6)  = strength of V_coul
crl  xful( ) = Linear Confining + Spin-orbit + Tensor (see FNOSCS)

ham = ham - real((jjval+1)*iphsav)
   &        *wiga*wigb*(gfulnn(indx)*hamclie
   &        + str(3)*cful(indx)*hamcle
   &        - hamcle*
   &          (str(5)*rful(indx)+str(12)*rful2(indx))
   &        + str(6)*q1q2*cful(indx)*hamclie
   &        - hamcle*xful(indx)  )

 70    continue

    go to 320

    endif

crl  Test for q-qbar or different flavors of q-q or qbar-qbar
      if(ibary.eq.0.or.mmtt.eq.0)then

crl  Insert for direct management of isospin phase
crl  Since mmtt = 0 here, product of two clebsch gordan coeffs
crl  is negative only when ordering of isospin projections is
crl  different in the two coefficients and when T = 0.
        phstx = +1.0
        if(itz2a.ne.itz2c) phstx=-1.0

    do 125 it = 1,2
      if(nimj(it).eq.0)go to 125

      jval = j(it)-jde
      hamt = 0.0
      strT0 = (1.d0-(-1.d0)**it)/2.d0
      strT1 = (1.d0-(-1.d0)**(it-1))/2.d0

crl  Test print
crl       if(iproc.eq.0)write(8,*) 'it, jde, jval, nimj',
crl   &           it, jde, jval, nimj(it)
```

```
      do 120 ij = 1,nimj(it)
        jval = jval + jde
        indx = indx + 1
        jjval = jval + jval
        if(IABS(mmjj).gt.jjval)go to 120

        wiga = wig3jr(j2a,j2b,jjval,m2a,m2b,-mmjj)
        wigb = wig3jr(j2c,j2d,jjval,m2c,m2d,-mmjj)

hamt = hamt + real(jjval+1)
   &        *wiga*wigb*(gfulnp(indx)*hamcli
   &        + str(3)*cful(indx)*hamcl
   &        + hamcl*
   &          (str(5)*rful(indx)+str(12)*rful2(indx))
   &        + str(6)*q1q2*cful(indx)*hamcli
   &        - hamcl*xful(indx)  )

 120    continue

crl  Manage an isospin Clebsch-Gordon arising since isospin
crl  projections are not organized by class in this quark application.
crl  Change of phase occurs only for T=0 matrix elements when ordering
crl  is different in the bra and ket
       phst = +1.0
       if(it.eq.1)phst = phstx

cr   Temporary management of flavor diagonality of Trel etc operators
       if(itz2a.ne.itz2c.or.itz2b.ne.itz2d) phst = 0.0
crl  End insert to manage interchange of isospin proj

       ham = ham + hamt * 0.5 * phst * real(iphsav)

 125  continue
     go to 320
     endif

crl   Test for q-q of the same flavor:
       if(ibary.eq.2.and.iabs(mmtt).eq.2)then
       if(nimj(2).eq.0)go to 320
       indx = indx + nimj(1)

       jval = j(2)-jde
       do 220 ij = 1,nimj(2)
         jval = jval + jde
         indx = indx + 1
```

```
        jjval = jval + jval
        if(IABS(mmjj).gt.jjval)go to 220

        wiga = wig3jr(j2a,j2b,jjval,m2a,m2b,-mmjj)
        wigb = wig3jr(j2c,j2d,jjval,m2c,m2d,-mmjj)

crl  str(3)  = strength of V_oge term
crl  str(5)  = strength of S=1 delta function
crl  str(12) = strength of S=0 delta function
crl  str(6)  = strength of V_coul
crl  xful( ) = Linear Confining + Spin-orbit + Tensor (see FNOSCS)
ham = ham + real((jjval+1)*iphsav)
   &        *wiga*wigb*(gfulpp(indx)*hamcli
   &        + str(3)*cful(indx)*hamcl
   &        - hamcl*
   &          (str(5)*rful(indx)+str(12)*rful2(indx))
   &        + str(6)*q1q2*cful(indx)*hamcli
   &        - hamcl*xful(indx)  )

 220    continue

      if(id(itrack(ii), icount(ii),11).ne.
   &    id(itrack(jj), icount(jj),11))go to 320

crl  Compute/add exchange term for identical particle case
crl  Antisymmetrization is the simple difference of a direct
crl  and an exchange matrix element.

    n(3) = ntrans(ll)
    n(4) = ntrans(kk)
    call fnoscs

    iphsav = iphsb**((j2a+j2b)/2) * iphsk**((j2c+j2d)/2)

    indx = indx - 1

      if(nimj(2).eq.0)go to 320
      indx = indx + nimj(1)

      jval = j(2)-jde
      do 270 ij = 1,nimj(2)
        jval = jval + jde
        indx = indx + 1
        jjval = jval + jval
        if(IABS(mmjj).gt.jjval)go to 270
```

```
      wiga = wig3jr(j2a,j2b,jjval,m2a,m2b,-mmjj)
      wigb = wig3jr(j2d,j2c,jjval,m2d,m2c,-mmjj)


crl  str(3)  = strength of V_oge term
crl  str(5)  = strength of S=1 delta function
crl  str(12) = strength of S=0 delta function
crl  str(6)  = strength of V_coul
crl  xful( ) = Linear Confining + Spin-orbit + Tensor (see FNOSCS)

ham = ham - real((jjval+1)*iphsav)
   &       *wiga*wigb*(gfulpp(indx)*hamclie
   &       + str(3)*cful(indx)*hamcle
   &       - hamcle*
   &         (str(5)*rful(indx)+str(12)*rful2(indx))
   &       + str(6)*q1q2*cful(indx)*hamclie
   &       - hamcle*xful(indx)  )

 270    continue

    endif

 320  ham = ham * phsj
    haml = haml * phsj

crl     if(n(1).eq.n(2))ham = ham*sq2
crl     if(n(3).eq.n(4))ham = ham*sq2

    if(ibary.eq.0)go to 1900

    fac1 = 1.0

 1890   ham = fac1*ham

 1900   continue

haml(7) = str(7) * (float(iidrct)*hamcld - float(iiexch)*hamcle)
    ham = ham + haml(7)
cjvv
crl  The following pseudo 2-body operator = direct product of
crl  1-body operators may be evaluated via the sps indexing of
crl  MFD directly, without information from FNOSCS.  Ordering
crl  convention of MFD MB states is sufficient to guarantee the
crl  following test finds all contributions.
```

```
crl  HOWEVER, once color introduced explicitly, we now manage
crl  antisymmetriztion for qq and qbar-qbar directly in MFD meaning
crl  original MFD ordering conventions were replaced with allowance
crl  of more general orderings.
     xnzfc=0.0
     if(ii.eq.kk.and.jj.eq.ll)then
     xnzfc=hamcli
     go to 350
     endif
crl  Handle the exchange case of 1-body operator as pseudo 2-body operator
crl  by explicitly inserting a minus sign.
     if(ii.eq.ll.and.jj.eq.kk)then
     xnzfc=-hamclie
     go to 350
     endif
c12c Following may be needed in mnop=3 usage
     if(mnop.eq.3.and.ii.eq.ll.and.jj.eq.kk)go to 350
c12c
 340 continue

     if(iverb8.ge.5.and.iproc.eq.0)then
     write(8,345) ii, jj, kk, ll, ham
 345 format(' In Function Ham - result', 4i5, e16.8)
     endif

crl  Prepare for cases with odd numbers of SU(2) flavor anti-downs.
     if(itz2a.eq.1.and.id(itrack(ii),icount(ii),11).eq.-1)ham = -ham
     if(itz2b.eq.1.and.id(itrack(jj),icount(jj),11).eq.-1)ham = -ham
     if(itz2c.eq.1.and.id(itrack(kk),icount(kk),11).eq.-1)ham = -ham
     if(itz2d.eq.1.and.id(itrack(ll),icount(ll),11).eq.-1)ham = -ham
     Return
 350 continue
     ham = ham + str(4)*hbomeg*(2.*nnc+llc + 2.*nnd+lld + 3.)*xnzfc/real(ifermi-1)

     go to 340
     end
```

ACKNOWLEDGEMENTS

I owe many debts of gratitude to several people that made important contributions to my research in recent years. Foremost is my academic advisor, James Vary, who has been extremely kind and generous with his time, guidance, effort and encouragement. The old adage that says a graduate thesis is research undertaken by a professor under particularly trying circumstances is certainly no truer than in my case.

I would also like to thank John Spence who provided many valuable discussions over the last several years. Most of them involved disabusing a stubborn graduate student of his naivete regarding things that are impossible or just plain wrong. That, above all, is a valuable service that cannot be dismissed.

Oleksiy Atramentov also merits more than just honorable mention. He has kindly provided me the results of some of his efforts to implement 1 and 2-body correlation functions, and as a consequence, we are in a much better position to ascertain the physical structure of the systems we have chosen to study. Indeed, his contribution is an indispensable tool, and I shall not forget it.